Initial mechanisms for the unimolecular decomposition of electronically excited nitrogen-rich energetic materials with tetrazole rings: 1-DTE, 5-DTE, BTA, and BTH

Bing Yuan and Elliot R. Bernstein

Citation: The Journal of Chemical Physics **144**, 234302 (2016); doi: 10.1063/1.4953552
View online: http://dx.doi.org/10.1063/1.4953552
View Table of Contents: http://aip.scitation.org/toc/jcp/144/23
Published by the American Institute of Physics

Initial mechanisms for the unimolecular decomposition of electronically excited nitrogen-rich energetic materials with tetrazole rings: 1-DTE, 5-DTE, BTA, and BTH

Bing Yuan and Elliot R. Bernstein[a)]
Department of Chemistry, Colorado State University, Fort Collins, Colorado 80523-1872, USA

(Received 29 January 2016; accepted 25 May 2016; published online 15 June 2016)

Unimolecular decomposition of nitrogen-rich energetic molecules 1,2-bis(1H-tetrazol-1-yl)ethane (1-DTE), 1,2-bis(1H-tetrazol-5-yl)ethane (5-DET), N,N-bis(1H-tetrazol-5-yl)amine (BTA), and 5,5'-bis(tetrazolyl)hydrazine (BTH) has been explored via 283 nm two photon laser excitation. The maximum absorption wavelength in the UV-vis spectra of all four materials is around 186–222 nm. The N_2 molecule, with a cold rotational temperature (<30 K), is observed as an initial decomposition product from the four molecules, subsequent to UV excitation. Initial decomposition mechanisms for these four electronically excited isolated molecules are explored at the complete active space self-consistent field (CASSCF) level. Potential energy surface calculations at the CASSCF(12,8)/6-31G(d) level illustrate that conical intersections play an essential role in the decomposition mechanism. The tetrazole ring opens on the S_1 excited state and through conical intersections $(S_1/S_0)_{CI}$, N_2 product is formed on the ground state potential energy surface without rotational excitation. The tetrazole rings of all four energetic molecules open at the N1—N2 ring bond with the lowest energy barrier: the C—N bond opening has higher energy barrier than that for any of the N—N ring bonds. Therefore, the tetrazole rings open at their N—N bonds to release N_2. The vibrational temperatures of N_2 product from all four energetic materials are hot based on theoretical calculations. The different groups (CH_2—CH_2, NH—NH, and NH) joining the tetrazole rings can cause apparent differences in explosive behavior of 1-DTE, 5-DTE, BTA, and BTH. Conical intersections, non-Born-Oppenheimer interactions, and dynamics are the key features for excited electronic state chemistry of organic molecules, in general, and energetic molecules, in particular. *Published by AIP Publishing.* [http://dx.doi.org/10.1063/1.4953552]

I. INTRODUCTION

This study focuses, both experimentally and theoretically, on determination of the initial decomposition reaction, activated by electronic excitation, for four nitrogen rich tetrazole based, isolated, energetic molecules in the gas phase. In this context energetic molecules are those that form a crystal of a condensed phase energetic material.[1–3]

Traditional energetic materials release their stored energy from oxidation of a carbon backbone (e.g., TNT, RDX, and HMX) or from cage-strain (e.g., 4,10-dinitro-2,6,8,12-tetraoxa-4,10-diazaisowurtzitane (TEX) and CL-20).[4–7] They are toxic, carcinogenic, and hazardous and most of these nitro and/or nitramine related explosives are polluting, with a high sensitivity to shock and friction.[4–7] Replacement of these nitro and nitramine energetic compounds by greener, safer alternatives with higher explosive or propellant performance is one of the main goals for current energetic materials research.[5,8,9]

Different from classical explosives, nitrogen-rich energetic materials store most of their energy in the form of high positive heats of formation (ΔH_f) and are, therefore, one of the ideal candidates for next generation energetic materials.[5,10] The decomposition of these compounds results predominantly in generation of N_2, which renders them friendly to the environment.[7] Such decompositions are accompanied by an enormous energy release due to the wide difference in the average bond energies of N—N (160 kJ/mol) and N=N (418 kJ/mol), compared to that of N≡N (954 kJ/mol).[5,10] Nitrogen rich compounds based on tetrazole rings are used as energetic materials. These species have intra-/inter-molecular N—H···H hydrogen bonds and π—π stacking interactions between adjacent tetrazole rings in arrays for high density: they occupy ideal middle ground for thermal and physical stability versus performance (stored energy density).[7,11]

The four high nitrogen content energetic molecules with two tetrazole rings in the structures studied in this work are 1,2-bis(1H-tetrazol-1-yl)ethane (1-DTE), 1,2-bis(1H-tetrazol-5-yl)ethane (5-DET), N,N-bis(1H-tetrazol-5-yl)amine (BTA), and 5,5′-bis(tetrazolyl)hydrazine (BTH). The molecular structures of these four energetic molecules are shown in Figure 1. With a nitrogen content of 67 w%,[12] 1-DTE and 5-DTE have two tetrazole rings linked by a flexible CH_2—CH_2 group:[11] in 1-DTE, the CH_2—CH_2 group connects the two N atoms beside the C atoms on the two tetrazole rings; and in 5-DTE, this bridge connects the two C atoms in the two tetrazole rings. Both molecules compose

a)Author to whom correspondence should be addressed. Electronic mail: erb@lamar.colostate.edu

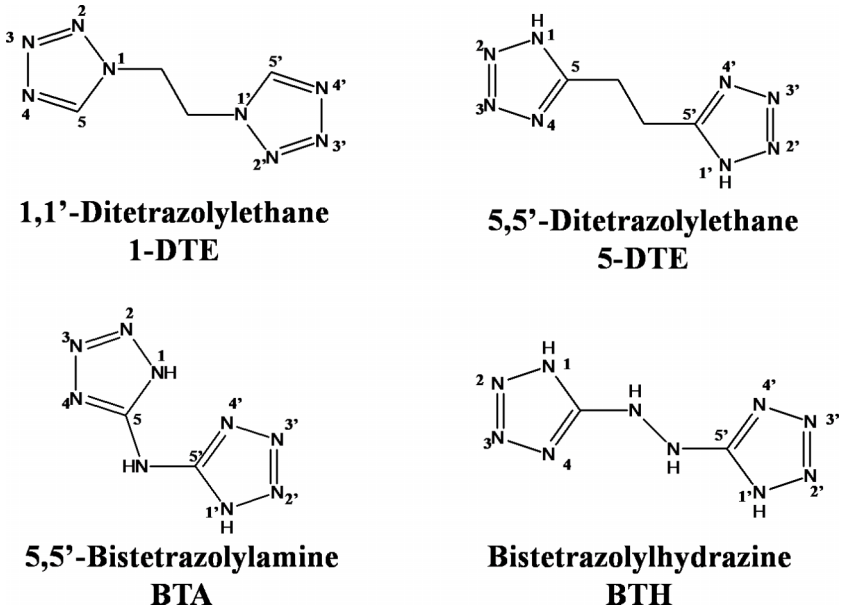

FIG. 1. Chemical structures of 1-DTE, 5-DTE, BTA, and BTH with atoms numbered for the rings.

environmental friendly explosives and gas generators with moderate explosion properties without toxic azide, nitro, or nitramine groups.[12] The decomposition temperatures of 1-DTE and 5-DTE compounds are ca. 200 °C and their friction sensitivity is greater than 360 N (TNT > 353 N, RDX > 120 N) with impact sensitivity >40 J (TNT > 15 J, RDX > 7.5 J).[12,13] The detonation velocity of 1-DTE is 7219 m/s, higher than that of TNT (7176 m/s), but lower than that of RDX (8800 m/s).[12]

BTA is an amine substituted with two tetrazole rings. The two tetrazole rings can rotate with respect to the plane of the —C—NH—C— amine group by 180°.[10] Neutral BTA possesses high thermal and mechanical stability with a high nitrogen content (82.34 w%).[14,15] It is considered to be an interesting nitrogen-rich framework for energetic salts because of its multi-proton donor sites with three reversible types of protonated and deprotonated analogues: BTA, BTA^-, and BTA^{2-}.[14–17] The decomposition temperature of BTA is ca. 250 °C, with friction sensitivity >360 N and impact sensitivity >30 J.[9] Its detonation velocity is 9120 m/s, which offers a greater explosive performance than that for RDX.[9]

With a nitrogen content of 83.3 w%,[7,18] the two tetrazole rings of BTH are linked by a flexible NH—NH group. Mass spectrometry measurements of BTH show that N_2 is the major decomposition gas.[7] BTH shows some decomposition after heating to ~170 °C for 6 h and its decomposition temperature is reported to be 208 °C.[7,19] The denotation velocity of BTH is 8523 m/s,[19] a little bit less than the value for RDX, with a friction sensitivity >360 N and an impact sensitivity >30 J.[7] All these four energetic materials show promising detonation parameters and they have lower friction and impact sensitivity compared to traditional energetic compounds which make them much safer in application.

Two directions have been pursued for explication of the release of stored energy from energetic materials: study of the sensitivity, heat of formation, and detonation velocity in the solid state and study of the initial bond dissociation reaction and decomposition mechanisms for the exothermic unimolecular chemical reactions driving detonation.[3,20] The latter approach emphasizes the isolated energetic molecule behavior as the essential first step in the energy release processes in either phase: this approach has been the one we have pursued over the last decade.[21–36] It can be justified by the local nature of the molecular excitation processes that occur upon even gentle shock wave excitation in any organic molecular solid, as discussed below.[37–39] Thus, similar to our previous work, we study the decomposition of isolated electronically excited energetic materials experimentally and calculate the decomposition mechanisms for a single energetic molecule theoretically, as is the approach pursued for many decades with regard to kinetic/mechanistic research.[21–36] In general, the difference between condensed phase and gas phase reactions is that solid state reactions occur within the rigid constraining environment of a crystal lattice, in which intermolecular interactions can influence reaction mechanisms and directions.[39] Other important factors that can affect the solid reactions include the presence of solvates, planar defects, phase transitions, disorder, and even crystal morphology.[39] Although condensed phase reactions can be more complicated than gas phase ones, studies of the unimolecular behavior of explosives enable researchers to understand initial decomposition mechanisms; moreover, they provide useful information toward the design of new energetic materials with low sensitivity and high detonation performance.[3,40] Recent DFT calculations explore the kinetics and thermodynamics for ground state decomposition of nitro-based energetic materials and molecules, highlighting the expectations for isolated molecule vs. condensed phase final product distributions.[41]

Energetic materials are sensitive to stored energy release initiation by heat, electrostatic discharge, impact, friction, shock, and laser irradiation.[42] The breaking of the first bond in an explosive molecule starts the exothermic, potentially

explosive reaction;[40,41] however, in which way the input energy can be concentrated to create sufficient energy to break an intramolecular bond is still a very complicated problem.[42] Mechanisms have been proposed involving shock waves passing through an energetic solid that result in considerable intramolecular vibrational excitation, which leads to bond rupture in a high energy molecule: this is referred to as a multiphonon-vibron up-pumping mechanism.[42,43] In our studies, we have followed decomposition mechanisms starting from excited molecular electronic states. Based on the centuries old observations of triboluminescence (TL, the emission of light from a solid generated by application of gentle mechanical stresses including electrification, pressure induced compression, thermal shock, hand grinding, and chemical reaction), one readily concludes that molecular electronic excitation must contribute to the initial chemical reactions that begin the release of stored molecular energy for an energetic system.[44–50] Consequently, our studies focus on the unimolecular decomposition mechanisms for electronically excited molecules comprising energetic materials. Both experiments and theory are explored in order to explicate the kinetics of and mechanisms for these initial processes.

The isolated molecule experiments and theory represent a reasonable approximation to the primary, initial behavior for the decomposition of energetic molecules in general condensed phase materials. Non-Born-Oppenheimer approximation conical intersections between zero order, adiabatic electronic states play a key role in the ultrafast (<100 fs) decomposition pathways.[21–23,51–54] The presented discussion includes product energy distribution, at the initial ultrafast molecular level, following electronic excitation for the isolated energetic molecule of interest. Determination of decomposition reaction mechanisms, kinetics, and dynamics for these large energetic molecules energized to excited electronic states (by shocks, arcs, sparks, light, etc.) emphasizes the importance of fundamental chemical physics to the technological advance of newly synthesized energetic materials, energy storage systems, and fuels.

In sum, in this work, energy resolved spectra of the initial product molecule N_2 are studied to define the initial decomposition dynamics of the energetic material isolated molecule through elucidating the rotational temperature of the N_2 product. Potential energy surfaces for the excited and ground electronic states are explored theoretically employing quantum chemistry calculations (Gaussian 09, CASSCF). The detailed decomposition mechanisms of 1-DTE, 5-DET, BTA, and BTH are thereby determined and discussed. As none of these energetic species contains an NO_2 or an N_2O_2 group, ring opening decomposition mechanisms are proposed. The difference of energy barriers for the tetrazole ring open via the C—N bond and N—N bond is compared. A detailed explication of the decomposition mechanisms for these energetic species is provided. These studies are both fundamental and practical as they make advances toward the application of fundamental chemical physics specifically to the behavior of new organic, energy storage materials.

II. EXPERIMENTAL PROCEDURES

The experimental setup consists of a matrix-assisted laser desorption (MALD) system, a supersonic jet expansion nozzle, and a time of flight mass spectrometer. Details of the instrumental design are described in our previous papers.[22,23] The nozzle used for the molecular beam generation is constructed from a Jordan Co. pulsed valve and a laser ablation attachment. The laser desorption head is attached to the front of the pulsed valve with three significant parts: (1) a 2×60 mm channel for the expansion gas from the nozzle, (2) a conical channel (3 mm at the outside and 1 mm at the intersection with gas expansion channel) for the ablation laser beam perpendicular to the expansion gas channel, and (3) a 40 mm diameter hole for the sample drum. The sample drum fits into the 40 mm hole and is simultaneously rotated and translated by a motor and gear system in the vacuum in order to present a fresh sample region to the ablation laser for each pulse. The nonvolatile samples are desorbed from the drum by 532 nm ablation laser, entrained in the flow of He carrier gas under a pressure of 80 psi through the 2×60 mm channel in the laser desorption head and expanded into the vacuum chamber. With 80 psi He backing pressure for the closed pulsed valve, the chamber pressure remains 8×10^{-8} Torr; with the valve open at 10 Hz, the chamber pressure increases to 4×10^{-7} Torr.

All sample drums for MALD are prepared by wrapping a piece of porous filter paper around a clean Al drum. A solution of 0.02 mol/l matrix (Rhodamine 6G) and 0.02 mol/l sample in water is uniformly sprayed on the drum surface while it is rotating under a halogen heat lamp in a fume hood to make sure the sample coating is dry. Rhodamine 6G is chosen because it has an intense absorption at 532 nm; consequently, it can efficiently absorb the 532 nm laser photons, and decompose. This process expels the intact energetic molecules, trapped in the dye matrix, into the supersonic expansion gas flow from the pulsed nozzle. An air atomizing spray nozzle (Spraying System Co.) with siphon pressure of 10 psi is used to deposit sample plus matrix on the filter paper surface. The dried drum with well-distributed sample is then placed in the laser ablation head assembly and put into the vacuum chamber for decomposition reaction studies. All four samples are supplied by Professor Thomas M. Klapökte, Ludwig-Maximilian University of Munich.

In addition to the ablation laser, one or two other lasers are required to photo-excite the sample in the beam and then detect the dissociated fragments. Laser ablation of any molecule will generate both ionic and neutral species. In our apparatus, only the neutrals can enter the electric field extraction/ionization region because the plates are continuously charged to 4.0 kV and 3.75 kV, as is usual for a linear 1 m time of flight mass spectrometer with a 3 plate ion focusing region for laser ionization of neutrals. Negative ions entering this region are attracted to the high voltage plate and are not deflected toward the flight tube/detector, and positive ions undergo a curved deflection as they enter the high voltage field region and do not reach the microchannel detector at all or are dispersed by the field to generate only a background signal, which is known to be quite small (<1 mV) by measurement.

A single pump/probe laser is used at 283 nm for sample initiation and N_2 detection following a one color (2 + 2) resonance-enhanced four photon ionization (REMPI) scheme [$a^1\Pi_g(v' = 1) \leftarrow X^1\Sigma_g(v'' = 0)$ and $I \leftarrow a$ transitions] through time of flight mass spectrometry (TOFMS).[55–57] Note that the energetic sample is in a condensed phase (1-DTE, 5-DTE, BTA, or BTH trapped in an R6G matrix) under 532 nm laser ablation, while for the 283 nm excitation/decomposition processes, it is in the form of an isolated energetic molecule. The UV 283 nm laser wavelengths for this process are generated by a dye laser, pumped by the second harmonic (532 nm) of a Nd: yttrium aluminum garnet laser's fundamental output (1.064 μm), in conjunction with a frequency doubling system. As four photons are required in one detection, the typical pulse energy of the UV laser is about 6-7 mJ/pulse, giving an intensity of $\sim 2.4 \times 10^9$–2.8×10^9 W/cm^2 for a 8 ns pulse duration. The molecular beam is perpendicularly crossed by the UV laser beam, which is focused to a spot size of about 0.2 mm diameter at the ionization region of the TOFMS. Before the detection of energetic materials, a 3% N_2 in He gas mixture is prepared and studied for calibration of the N_2 rotational spectrum.

The timing sequence of pulsed nozzle, ablation laser, and excitation/ionization laser is controlled by time delay generators (SRS DG535). The experiment is performed at a repetition rate of 10 Hz. Ion signals in the TOFMS are detected by a microchannel plate (MCP) and signals are recorded and processed on a personal computer (PC) using an ADC card (Analog Devices RTI-800) and a boxcar averager (SRS SR 250).

Since no experimental data exist for vertical excitation energies of 1-DTE, 5-DTE, BTA, and BTH molecules, in order to determine the accuracy of theoretical calculation for the higher electronic states, the experimental UV-vis absorption spectra of these four energetic materials are taken with an UV-vis-NIR Varian Cary 500 spectrometer in the range from 182 nm to 1000 nm. The four samples are dissolved in water with concentrations between 10^{-6} and 10^{-5} mol/l. These spectra are discussed in Section IV.

III. COMPUTATIONAL METHODS

Most calculations are executed at the CASSCF(12,8)/6-31G(d) level of theory within the Gaussian 09 program. To explore the excited state potential energy surfaces, the active space comprises 12 electrons distributed in 8 orbitals, denoted as CASSCF (12,8). No symmetry restrictions are applied for the calculations. For the calculation of all four energetic molecules, equilibrium geometry calculations are conducted taking the total charge as neutral and the spin multiplicity as 1 (S = 0). Orbital plots are presented in Figures 2–5. Orbitals used for the 1-DTE and BTH active spaces are two π-bonding orbitals on one of the tetrazole rings $\pi_{1,\text{ring}}$ and $\pi_{2,\text{ring}}$, four σ-nonbonding orbitals on one of the tetrazole rings $n\sigma_1$, $n\sigma_2$, $n\sigma_3$, and $n\sigma_4$, and two π-antibonding orbitals on one of the tetrazole rings π_1^* and π_2^* as shown in Figures 2 and 5. Orbitals used for 5-DTE are similar to those of 1-DTE, except for one of the π-antibonding orbitals, which is located on the whole molecular system, not single tetrazole ring, as shown in Figure 3. Orbitals used for the BTA active space are shown in Figure 4. They include two π-bonding orbitals around the whole molecular system π_1 and π_2, one π-bonding orbital on one tetrazole ring π_{ring}, three σ-nonbonding orbitals around the whole molecular system $n\sigma_1$, $n\sigma_2$, and $n\sigma_3$, and two π-antibonding orbitals on the whole molecule π_1^* and π_2^*. For all four energetic materials, the decomposition path is a tetrazole ring opening channel; thus, both σ-nonbonding orbitals and π orbitals on the tetrazole ring are chosen for the reaction description. Chosen orbitals are molecular orbitals from HOMO-4 to LUMO + 2. Eight orbitals are selected because this is the maximum limit for CASSCF for conical

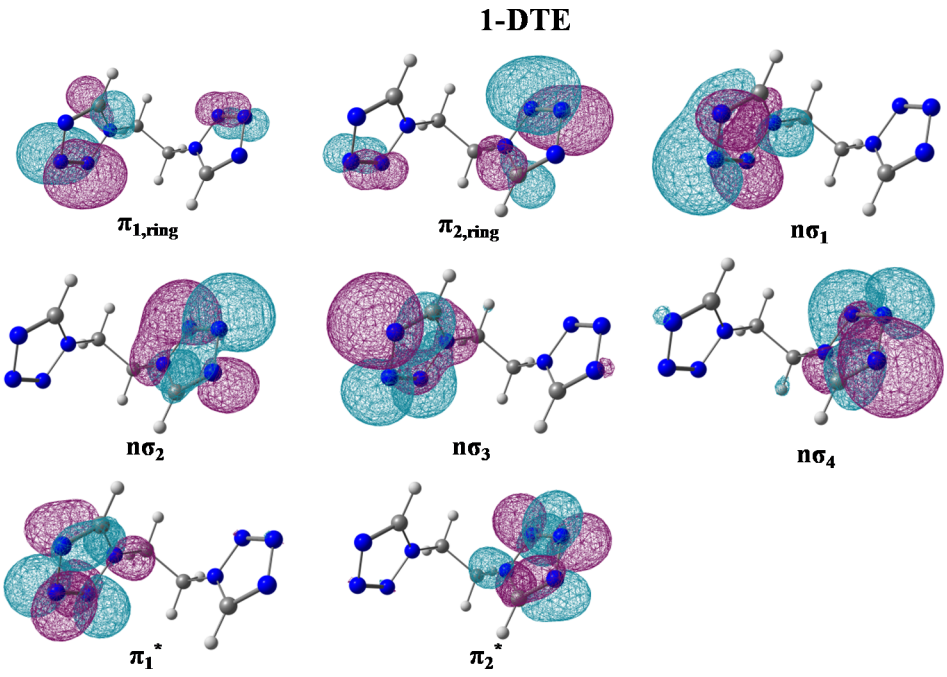

FIG. 2. Orbitals used in the active space of CASSCF calculations for 1-DTE. The (12,8) active space comprises two π-bonding orbitals ($\pi_{1,\text{ring}}$ and $\pi_{2,\text{ring}}$), four σ-nonbonding orbitals ($n\sigma_1$, $n\sigma_2$, $n\sigma_3$ and $n\sigma_4$), and two π-antibonding orbitals (π_1^* and π_2^*). For atoms in the structure, grey is carbon, blue is nitrogen, and white is hydrogen.

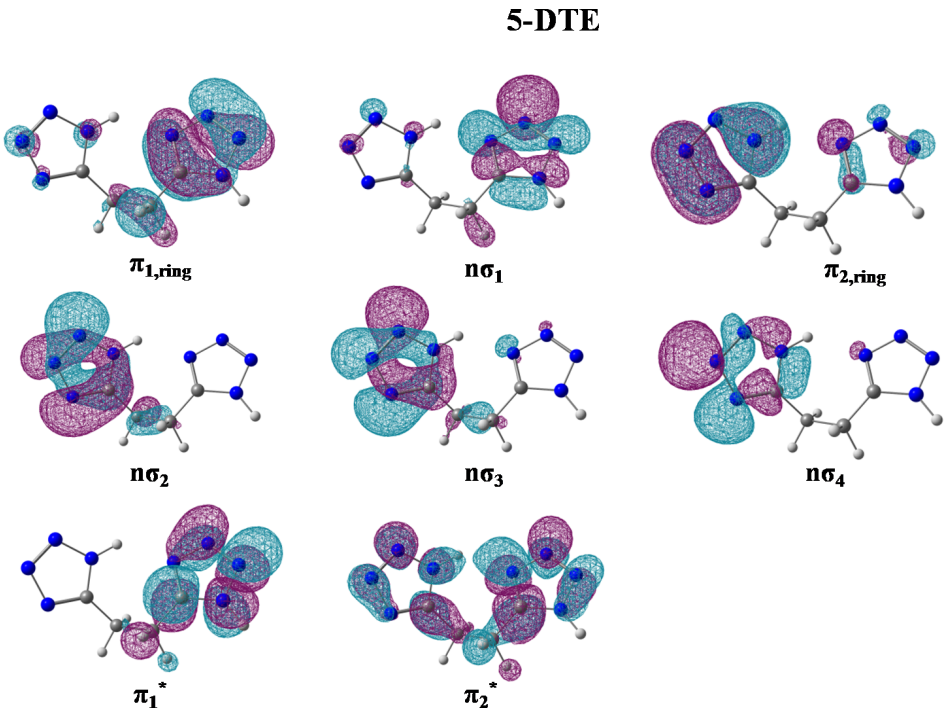

FIG. 3. Orbitals used in the active space of CASSCF calculations for 5-DTE. The (12,8) active space comprises two π-bonding orbitals ($\pi_{1,ring}$ and $\pi_{2,ring}$), four σ-nonbonding orbitals ($n\sigma_1$, $n\sigma_2$, $n\sigma_3$ and $n\sigma_4$), and two π-antibonding orbitals (π_1^* and π_2^*). For atoms in the structure, grey is carbon, blue is nitrogen, and white is hydrogen.

intersection calculations due to the need for analytic second derivatives. The agreement between theory and experiment demonstrates that the chosen 8 orbitals are sufficient in this instance.

Excitation energies are calculated by state averaging over the ground and excited states with equal weights for each state. Larger basis sets than 6-31G(d) for CASSCF calculations do not substantially improve the results and understanding of the reaction mechanisms.[24,25]

Critical points (minima and transition state structures) are characterized by analytical frequency calculations, and minimum energy paths are calculated using an intrinsic reaction coordinate (IRC) algorithm implemented in the Gaussian 09 program suite. To find the transition and intermediate states along the reaction pathways, a relaxed scan optimization algorithm as implemented is employed in which all geometrical parameters except for the specified bond distance are optimized and electronic energies are monitored as the specified bond is elongated. The bond length increase for each step is 0.1 Å for a total scan length of 2.5 Å. In the scan, the structure with peak potential energy is most likely a transition state, and the structure with potential energy in a valley is most likely an intermediate state. To verify this conclusion and obtain a more accurate potential energy

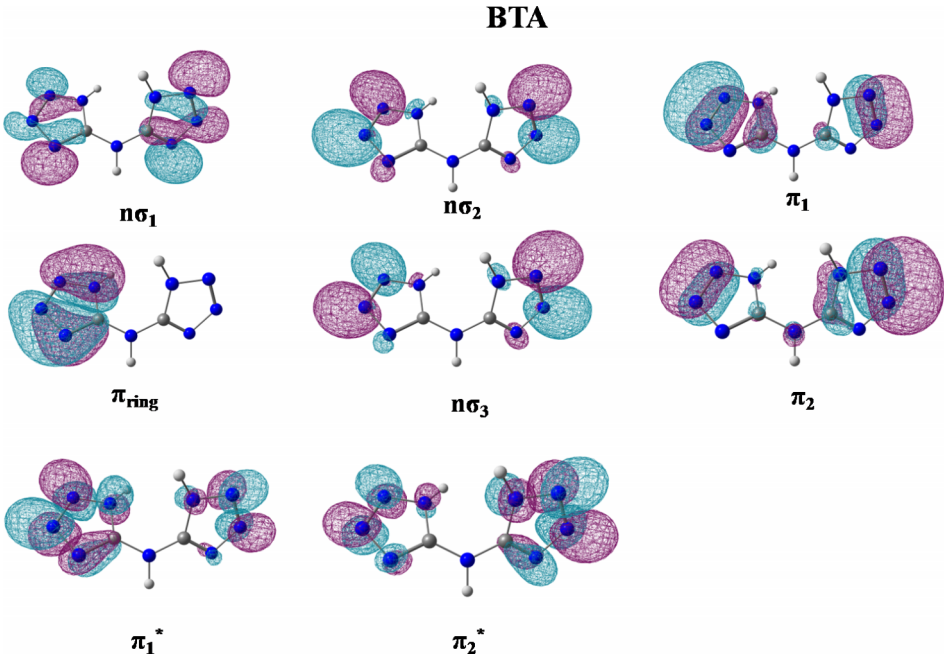

FIG. 4. Orbitals used in the active space of CASSCF calculations for BTA. The (12,8) active space comprises three π-bonding orbitals (π_{ring}, π_1 and π_2), three σ-nonbonding orbitals ($n\sigma_1$, $n\sigma_2$, and $n\sigma_3$), and two π-antibonding orbitals (π_1^* and π_2^*). For atoms in the structure, grey is carbon, blue is nitrogen, and white is hydrogen.

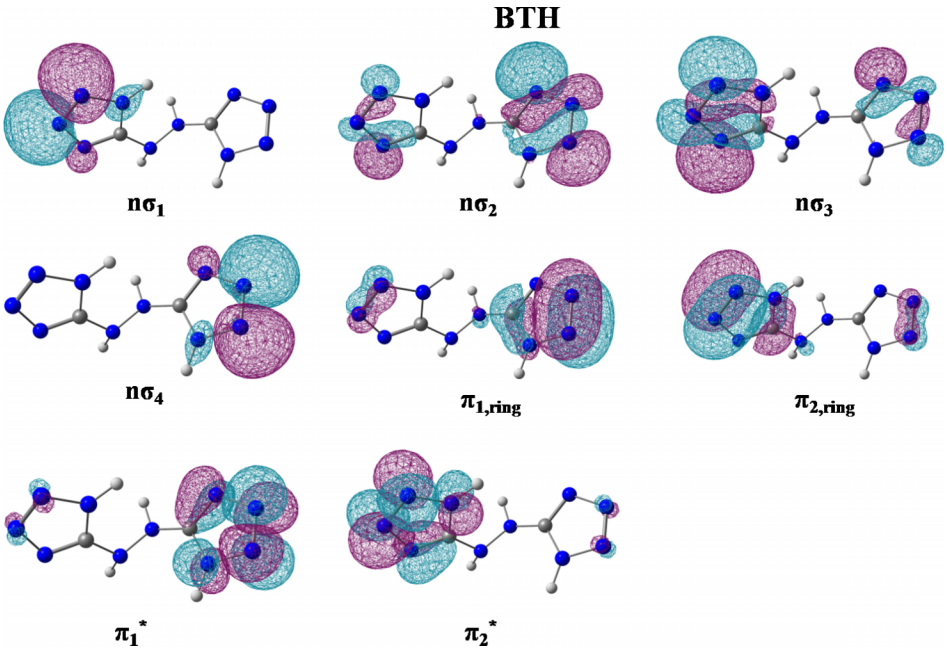

FIG. 5. Orbitals used in the active space of CASSCF calculations for BTH. The (12,8) active space comprises two π-bonding orbitals ($\pi_{1,ring}$ and $\pi_{2,ring}$), four σ-nonbonding orbitals ($n\sigma_1$, $n\sigma_2$, $n\sigma_3$ and $n\sigma_4$), and two π-antibonding orbitals (π_1^* and π_2^*). For atoms in the structure, grey is carbon, blue is nitrogen, and white is hydrogen.

surface for the transition/intermediate states, the molecular structure provided in the scan is used as the initial structure in the following optimization calculation with CASSCF(12,8) as the active space. In our previous study, the transition state structure on the first excited state S_1 between the minimum structure on $S_{1,min}$ and the conical intersections $(S_1/S_0)_{CI}$ is derived from the TD-DFT/6-31G(d) method;[25,26] however, in this work, we find the converged optimized transition state structures on the S_1 state using a CASSCF(12,8) method for all four energetic materials. Therefore, the calculational variations between the TD-DFT and CASSCF methods are avoided.

The accuracy of the calculations along the reaction pathway is difficult to estimate since experimental information about the conical intersections and the transition states is not available. Calculations presented in this paper, however, are based on the experimental observations including the decomposition product N_2 and its internal energy distribution. Thus, the proposed reaction pathways/mechanisms, based on the computational results, provide a reasonable, and at minimum qualitative, interpretation for the experimental observations.

IV. EXPERIMENTAL RESULTS AND DISCUSSION

A. UV-vis absorption spectra of 1-DTE, 5-DTE, BTA, and BTH

The UV-vis absorption spectra for 1-DTE, 5-DTE, BTA, and BTH are shown in Figure 6: the maximum absorption wavelengths in the experimental range for 1-DTE and 5-DTE are 187 and 186 nm, respectively. For BTA, there is a small absorption peak at 222 nm which is almost merged with the nearby absorption peak at 207 nm with much higher signal intensity. Similar to BTA, BTH has two absorption wavelengths at 212 nm and 187 nm, respectively; the 187 nm peak has higher intensity. In the decomposition study, the laser wavelength is 283 nm, which is lower in energy than the absorption wavelength; therefore, the excitation and decomposition of these four energetic materials occur through a two photon absorption. As N_2 detection is a one color, (2 + 2), resonance-enhanced, four photon ionization (REMPI) process, the laser energy/pulse is ca. 10-30 times greater than that employed for (1 + 1) REMPI detection, such as employed for NO. The overall excitation/N_2 detection process for 1-DTE, 5-DTE, BTA, and BTH is thereby a six photon process: this can be compared to the excitation/NO detection process for nitramines, which is a three photon process overall.

B. Decomposition product N_2

Decomposition product N_2 is observed from electronically excited 1-DTE, 5-DTE, BTA, and BTH compounds

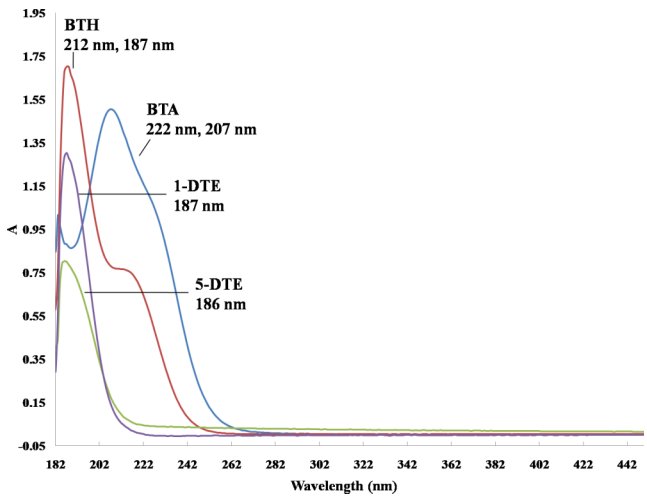

FIG. 6. UV-vis absorption spectra of 1-DTE, 5-DTE, BTA, and BTH with maximum absorption wavelengths. All four samples are dissolved in distilled water.

employing 283 nm excitation and TOFMS detection. The 283 nm excitation wavelength corresponds to the resonance (1-0) vibronic band of the $a^1\Pi_g \leftarrow X^1\Sigma_g$ electronic transition of the N_2 product. REMPI (2 + 2) rotationally resolved spectra of the N_2 product from these four energetic materials are obtained by scanning the laser excitation wavelength. The line width of the N_2 mass peak is 10 ns (the laser pulse width) and laser beam intensity is varied without change in the N_2 TOFMS line width. Excited electronic states of these four energetic materials, which might be generated in the ablation process, are effectively relaxed and cooled in the highly collisional expansion process, through the supersonic nozzle. Additionally, the 532 nm ablation laser is not directly resonant for these molecules and these photons are almost completely absorbed by the R6G matrix. These energetic materials have a very low absorption at 532 nm (2.33 eV): their higher electronic states are roughly 3–4 eV above this ablation photon energy. In the ablation process, energetic materials can be heated to higher rovibrational states of the electronic ground state. These intact energetic molecules are then cooled in the supersonic expansion. Based on our previous studies, decomposition of such energetic molecules under 532 nm laser irradiation is below our detection limit.[22]

Figure 7 shows the spectra of $a^1\Pi_g(v' = 1) \leftarrow X^1\Sigma_g(v'' = 0)$ rovibronic transition of the N_2 molecule arising from a 3% N_2/He mixture, and 1-DTE and 5-DTE compounds following excitation to their excited electronic states. The rotational spectra of N_2 from the N_2 gas mixture and the two energetic materials have similar patterns: the most intense peak in each spectrum of N_2 corresponds to the S_0 peak of the S branch rotational transitions. Other peaks, including S_1 and S_2 of the S branch, Q_1 peak of the Q branch, and P_2 of the P branch rotational transitions, are labeled in Figure 7.[56,57] The rotational spectrum of N_2 from 1-DTE clearly evidences three peaks of the S branch. S_0, S_1, and S_2 can be clearly

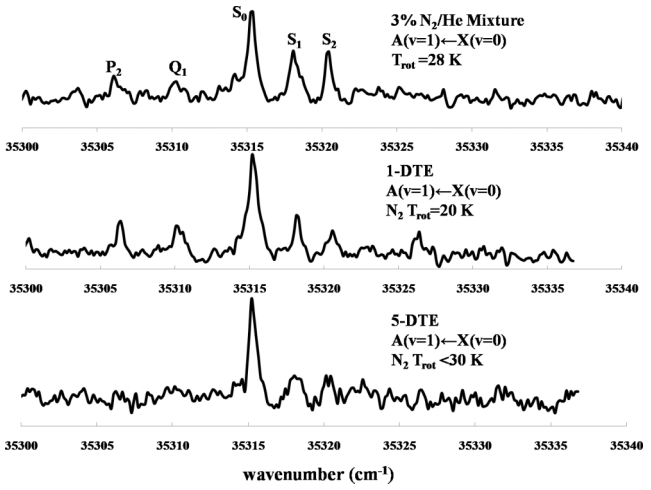

FIG. 7. One color (2 + 2) REMPI spectra of the vibronic transitions $a^1\Pi_g(v' = 1) \leftarrow X^1\Sigma_g(v'' = 0)$ of N_2 from 3% N_2/He mixture and from electronic state excitation of 1-DTE and 5-DTE. The rotational temperature of the 3% N_2 mixture calculated from a Boltzmann plot equals 28 K. The rotational temperatures of N_2 decomposition products from 1-DTE and 5-DTE (as indicated) are estimated to be smaller than 30 K.

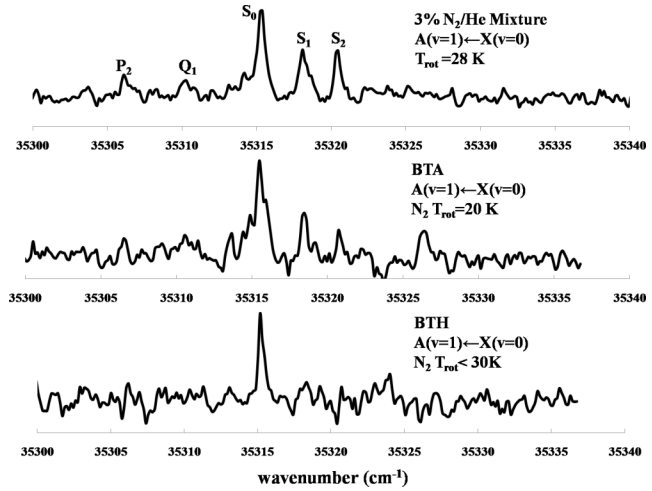

FIG. 8. One color (2 + 2) REMPI spectra of the vibronic transitions $a^1\Pi_g(v' = 1) \leftarrow X^1\Sigma_g(v'' = 0)$ of N_2 from 3% N_2/He mixture and from electronic state excitation of BTA and BTH. The rotational temperature of the 3% N_2 mixture calculated from a Boltzmann plot equals 28 K. The rotational temperatures of N_2 decomposition products from BTA and BTH (as indicated) are estimated to be smaller than 30 K.

observed. The rotational transitions of N_2 from 5-DTE are much weaker, and only the strongest S_0 peak is identified. The spectra of $a^1\Pi_g(v' = 1) \leftarrow X^1\Sigma_g(v'' = 0)$ rovibronic transition of the N_2 molecule arising from a 3% N_2/He mixture and BTA and BTH compounds are shown in Figure 8. S_0, S_1, and S_2 peaks are detected for the N_2 rotational spectrum derived from BTA, while for BTH dissociation, only the main S_0 peak of N_2 is observed. The rotational spectrum for the N_2/He mixture, 1-DTE, and BTA expansions are similar to that of previous studies, indicating an N_2 rotational temperature of about 20 K. Details of this calculation are published in a previous paper. The N_2 signals from 5-DTE and BTH are much less intense than those of the N_2 gas mixture and the other two energetic materials, as only the S_0 peak can be consistently observed in the N_2 rotational spectra. Therefore, through comparison to the spectrum of the N_2 gas mixture and previous studies,[25,26,58] the rotational temperatures of the N_2 product released from 5-DTE and BTH compounds are assigned only as lower than 30 K.

To find the vibrational temperature of the N_2 initial fragmentation product, the rotational spectra of N_2 should be obtained from several vibronic bands. The signal intensity of the reported N_2 rotational transition from ground rovibronic state $v'' = 0$ is ca. 80 mV, about 4 times higher than the noise level. To get N_2 rovibronic transition spectra starting at $v'' \geq 1$ of the ground electronic state, the signal intensity should be 5-10 times lower than the above 80 mV, assuming an established vibrational temperature, as is typical for such fragmentation processes.[22–36] This estimated transition intensity is well under the detection limit for the measurement. Consequently, further N_2 rovibronic bands were not obtained in these experiments, and thus vibrational temperature are not determined for the N_2 products of these molecules.

TOF mass spectra, obtained under 283 nm excitation employed especially for N_2 detection, display a few very weak additional features in the low mass region. These features are,

however, much weaker and their intensity remains constant as the excitation wavelength is scanned. These additional weak features are most likely not a result of a major decomposition pathway from any of the energetic molecules.

V. THEORETICAL RESULTS AND DISCUSSION

Experimental results yield that N_2 molecules are initial nanosecond electronic excitation decomposition product for the energetic systems explored under this study. In order to understand the experimental data more completely and derive reaction mechanisms, theoretical calculations of molecular geometries and energies for the Franck-Condon structures, conical intersections, transition states, and intermediate states along both the ground and excited state potential energy surfaces are performed for the four energetic materials. These theoretically derived reaction paths with potential energies and molecular geometries are shown in Figures 9-16.

Four possible decomposition mechanisms are explored for 1-DTE, 5-DTE, and BTA molecules in the theoretical study, through four different conical intersections between the S_1 and S_0 electronic states, all of which are related to four tetrazole ring position openings. Five possible decomposition mechanisms are explored for BTH, including four different tetrazole ring opening positions and the breaking of the C—N bond between one tetrazole ring and the NH—NH bridge between the rings. All these reaction channels are chosen because they are energy available and accessible for the creation of N_2 products. The actual reaction pathways used by these molecules will depend on different factors, for example, the rate of internal vibrational energy redistribution, the heights of reaction barriers, and the rate of non-adiabatic transition through the different conical intersections: at present these dynamics are not individually experimentally accessible.

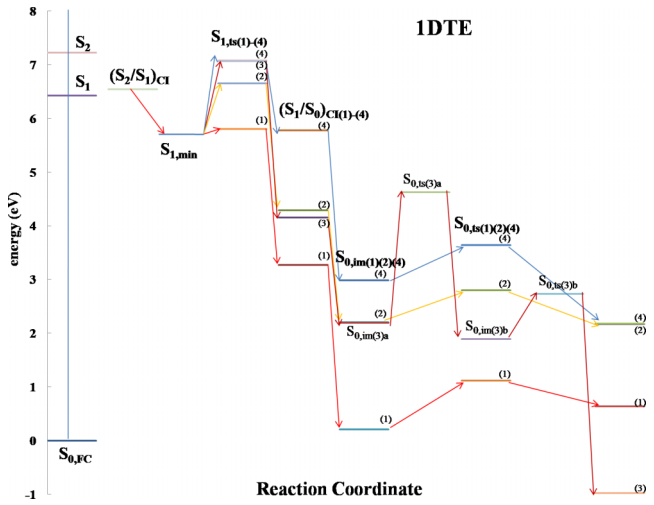

FIG. 9. A schematic one-dimensional projection of the multi-dimensional energy surfaces for four 1-DTE dissociation paths computed at the CASSCF(12,8)/6-31G(d) level of theory. The four reaction paths contain four tetrazole ring opening channels. The red, orange, brown, and blue arrows represent (1)–(4) different reaction channels for N_2 dissociation, respectively. $S_{0,FC}$ is the optimized minimum energy of 1-DTE on the S_0 state. $(S_1/S_0)_{CI(1)-(4)}$ are the conical intersections between the S_0 and S_1 states and (1)-(4) are related to different tetrazole ring opening positions (reactions, minimum energy coordinates) in different reaction channels. $S_{1,ts(1)-(4)}$ are the excited transition states on the S_1 electronic state surface between the minimum structure $S_{1,min}$ on S_1 and their related conical intersections. $S_{0,im(1)(2)(4)}$ and $S_{0,im(3)ab}$ are the intermediate states on the ground electronic state S_0 after $(S_1/S_0)_{CI(1)}$, and $S_{0,ts(1)(2)(4)}$ and $S_{0,ts(3)ab}$ are the transition states on the S_0 state following each intermediate state in the different reaction channels. $S_{0,n2(1)-(4)}$ are molecules with N_2 dissociated products on the S_0 state.

Calculations at the CASSCF(12,8)/6-31G(d) level are employed to determine the vertical excitation energies for 1-DTE, 5-DTE, BTA, and BTH compounds from the ground electronic state S_0 (FC structure) to the first and second excited electronic states S_1 and S_2. Under the chosen experimental conditions for these studies, the molecular excitation must be a two photon process: the energetic molecules can thereby be excited to an S_n electronic state. They rapidly (<100 fs) evolve to the ground electronic potential energy surface through conical intersections between the different electronic states. Since the exact pathways along which these molecules evolve from high electronic excited states to their S_1 excited states do not significantly affect the decomposition, only the S_1 excited and S_0 ground state reaction mechanisms are discussed below.

Since data are not available for vertical excitation energies of 1-DTE, 5-DTE, BTA, and BTH molecules, experimental UV-vis absorption spectra of these four energetic materials are obtained to determine the accuracy of the CASSCF calculations. The vertical excitations calculated through CASSCF(12,8)/6-31G(d) (12 electrons, 8 orbitals) for the first excited electronic state S_1 of 1-DTE and 5-DTE are 6.42 and 7.08 eV, respectively. The maximum absorption wavelengths for these two energetic materials in UV-vis absorption spectra shown in Figure 6 are 187 nm (6.63 eV) and 186 nm (6.67 eV), respectively. The commonly accepted uncertainty range for CASSCF calculated energies is ±0.5 eV: calculation of the relevant excited states of 1-DTE and 5-DTE is thus considered reasonable. The vertical excitations calculated through CASSCF(12,8)/6-31G(d) for the first and second excited electronic states S_1 and S_2 of BTH are 6.57 and 7.30 eV, respectively. The two absorption wavelengths of BTH in UV-vis absorption shown in Figure 6 are 212 nm (5.85 eV) and 187 nm (6.63 eV). The vertical excitations calculated through CASSCF(12,8)/6-31G(d) for the first and second excited electronic states S_1 and S_2 of BTA are 6.49 and 7.25 eV, respectively. The two absorption wavelengths of BTA in UV-vis absorption shown in Figure 6 are 222 nm (5.58 eV) and 207 nm (5.99 eV). The theoretical excited state (vertical) excitation energies for BTA and BTH are about 0.72–0.91 eV larger for the S_1 excited state than the experimental, peak absorption energies. The energy differences between these experimental and the theoretical results are larger than those for 1-DTE and 5-DTE, mainly because the molecular structures of BTA and BTH are tetrazole rings linked by NH or NH—NH group, while in 1-DTE and 5-DTE, it is CH_2—CH_2 group instead. In the BTA/BTH solutions, more hydrogen bonds can be formed, which cause a red-shift of the wavelengths in the UV-vis absorption spectra.[59,60] Calculation of excited state energies at the CASSCF(12,11) level for BTA yields the S_1 and S_2 state energies 6.30 and 6.92 eV, respectively, with no apparent improvement over CASSCF(12,8) results. Therefore, although a CASSCF(12,8) calculation is not a

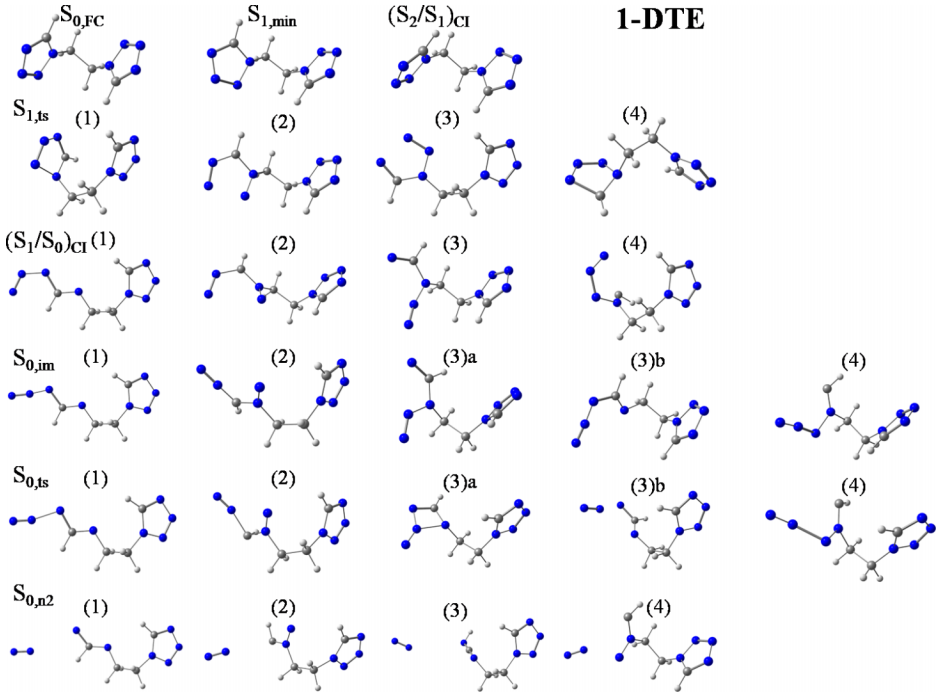

FIG. 10. Structures of all critical points and conical intersections mentioned in Figure 9 along the 1-DTE dissociation reaction paths (1)-(4). For atoms in the structure, grey is carbon, blue is nitrogen, and white is hydrogen.

perfect theoretical approach, it is apparently sufficient for the present mechanistic pathway and critical point identification on the S_1 and S_0 potential energy surfaces for 1-DTE, 5-DTE, BTA, and BTH energetic molecules.

From our previous studies,[24,25] enlarging the basis set does not significantly improve the relative excitation energies or critical point energies; therefore, a 6-31G(d) basis set is used for all calculations to maintain optimum conditions for computational cost, accuracy, and comparisons. Additionally, for the decomposition mechanisms of the four energetic materials, only molecular singlet states and singlet-singlet transitions are considered, because based on our previous femto-second studies of energetic molecules RDX and HMX,[23] the decomposition dynamics fall into the time scale of our excitation pulse duration (ca. 100 fs). These results emphasize that gas phase energetic material decomposition is an extremely fast non-adiabatic reaction at the molecular level. Molecular singlet-singlet transitions are much faster than singlet-triplet, spin forbidden transitions. The time scale of molecular fluorescence emission is between 10^{-5} and 10^{-10} s, while that for phosphorescence emission is 10^{-4} s to 10 s.[61] Therefore, singlet-triplet transitions and couplings are not the initial, main energy conversion pathway for these energetic systems.

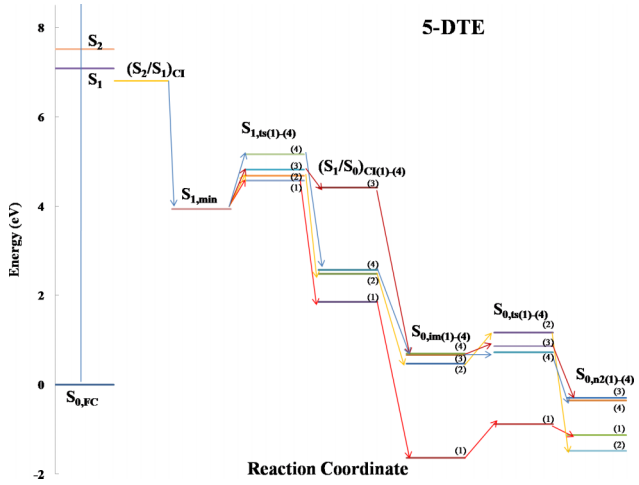

FIG. 11. A schematic one-dimensional projection of the multi-dimensional energy surfaces for four 5-DTE dissociation paths computed at the CASSCF(12,8)/6-31G(d) level of theory. The four reaction paths contain four tetrazole ring opening channels. The red, orange, brown, and blue arrows represent (1)–(4) different reaction channels for N_2 dissociation, respectively. $S_{0,FC}$ is the optimized minimum energy of 5-DTE on the S_0 state. $(S_1/S_0)_{CI(1)-(4)}$ are the conical intersections between the S_0 and S_1 states and (1)-(4) related to four conical intersections in different reaction paths. $S_{1,ts(1)-(4)}$ are the excited transition states on the S_1 surface between the minimum structure $S_{1,min}$ on the S_1 excited electronic state and the related conical intersections. $S_{0,im(1)-(4)}$ are the intermediate states on the S_0 state after $(S_1/S_0)_{CI(1)-(4)}$, and $S_{0,ts(1)-(4)}$ are the transition states on the S_0 surface following the intermediate states $S_{0,im(1)-(4)}$ in different reaction channels. $S_{0,n2(1)-(4)}$ are N_2 dissociated products on the S_0 surface.

A. Potential energy surfaces for 1-DTE

Schematic one-dimensional projections of the multidimensional singlet potential energy surfaces (S_0 and S_1) of 1-DTE, with locations and potential energies (the presented energies are not corrected for zero point energy) for different critical points and conical intersections along the minimum energy reaction paths, are plotted in Figure 9 and the energies for these points are summarized in Table I. Figures 9 and 10 described four different reaction channels (mechanisms) for 1-DTE decomposition. The reaction coordinates depicted in Figures 9 and 10 include C—N and N—N bond lengths within the tetrazole rings, either of which can be the active site for 1-DTE fragmentation: arrows with red, orange, brown, and blue colors in Figure 9 indicate different possible reaction channels for 1-DTE decomposition. The structures of each critical point and conical intersection are summarized in Figure 10. In Figures 9 and 10, FC geometry $S_{0,FC}$ is

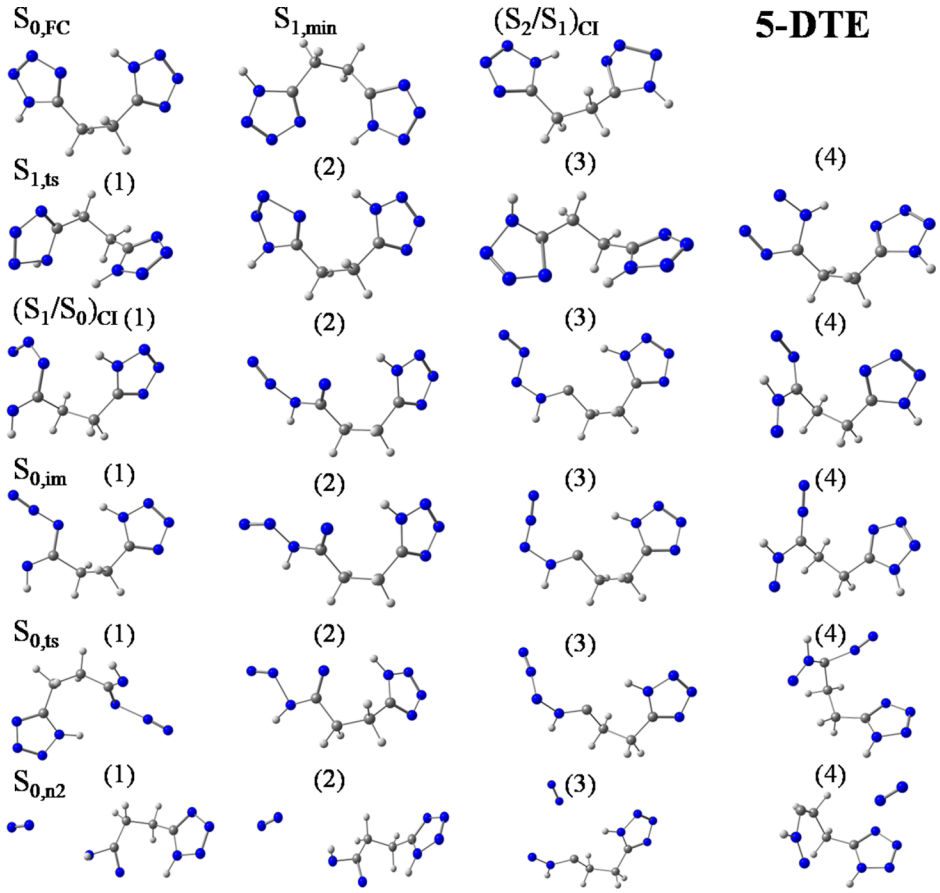

FIG. 12. Structures of all critical points and conical intersections mentioned in Figure 11 along the 5-DTE dissociation reaction paths (1)-(4). For atoms in the structure, grey is carbon, blue is nitrogen, and white is hydrogen.

the optimized minimum energy of 1-DTE on the S_0 state, $(S_1/S_0)_{CI(1)\text{-}(4)}$ are conical intersections between the S_0 and S_1 states: pathways (1)-(4) are related to different tetrazole ring opening positions in different reaction channels. $S_{1,ts(1)\text{-}(4)}$ are the excited transition states on the S_1 electronic state surface between the minimum structure $S_{1,min}$ on S_1 and their related conical intersections. $S_{0,im(1)\text{-}(4)}$ are the intermediate states on the ground electronic state surface S_0 after $(S_1/S_0)_{CI(1)}$. $S_{0,ts(1)\text{-}(4)}$ are the transition states on the S_0 state following each intermediate state ($S_{0,im(1)}$ to $S_{0,im(4)}$) of the different reaction channels. Of these channels, pathway (3) has two transition states $S_{0,ts(3)a}$ and $S_{0,ts(3)b}$ and two intermediate states $S_{0,im(3)a}$ and $S_{0,im(3)b}$ on the ground electronic state S_0 and subscripts (a) and (b) are labeled to distinguish them. $S_{0,n2(1)\text{-}(4)}$ are molecules with N_2 dissociated products on the S_0 state.

The reaction paths in Figure 9 show that with two photon absorption, 1-DTE can be excited to an S_n ($n > 2$) excited state: it then evolves to the first excited electronic state S_1 through several conical intersections among the different excited electronic states. As conical intersections between highly excited electronic states (S_n, $n > 2$) are typically not accurately calculated through a CASSCF algorithm, accurate energies for these conical intersections are not listed; however, the concept that molecules evolve from higher electronic states to lower electronic states through conical intersections is well documented in many studies.[21–36,51–54]

On the S_1 electronic excited state surface, 1-DTE undergoes a rapid internal conversion to the energy minimum structure $S_{1,min}$. Following this, the molecule encounters energy barriers for the transition states $S_{1,ts(1)\text{-}(4)}$, and moves to the ground electronic state through conical intersections $(S_1/S_0)_{CI(1)\text{-}(4)}$: molecules undergoing this process would place sufficient vibrational energy in the S_0 state, transferred from the S_1 (and S_n) electronic energy, to dissociate. Totally four transition states on the S_1 surface, related to four different conical intersections, are identified. The energies of these transition states are listed in Table I.

The reaction path with the lowest transition state energy shown in Figure 9 is the red one (reaction path (1) in Figure 9 and Table I). Along this reaction coordinate (red path), the 1-DTE molecule moves from $S_{1,min}$, surmounts a 0.31 eV energy barrier at $S_{1,ts(1)}$, and then reaches conical intersection $(S_1/S_0)_{CI(1)}$. Because the red path has the lowest energy barrier, this channel might be the most probable reaction path for the fragmenting system: the tetrazole ring opens at the N1—N2 bond (atoms labeled in Figure 1) along this coordinate.

The reaction path with the highest energy barrier from $S_{1,min}$ to $(S_1/S_0)_{CI(4)}$ shown in Figure 9 is the blue line (reaction path (4) in Figure 9 and Table I), which has a energy barrier of 1.57 eV through $S_{1,ts(4)}$, as the tetrazole ring opens between the C5—N4 bond. As all these energy barriers are energy available in the 2-photon absorption experimental system, all four reaction channels are reasonable. The other two reaction paths from $S_{1,min}$ through two conical intersections $(S_1/S_0)_{CI(2)}$ and $(S_1/S_0)_{CI(3)}$ are shown in Figure 9 as the orange (reaction path (2)) and brown (reaction path (3)) lines. The energy barriers to these two conical intersections are 1.15 and 1.56

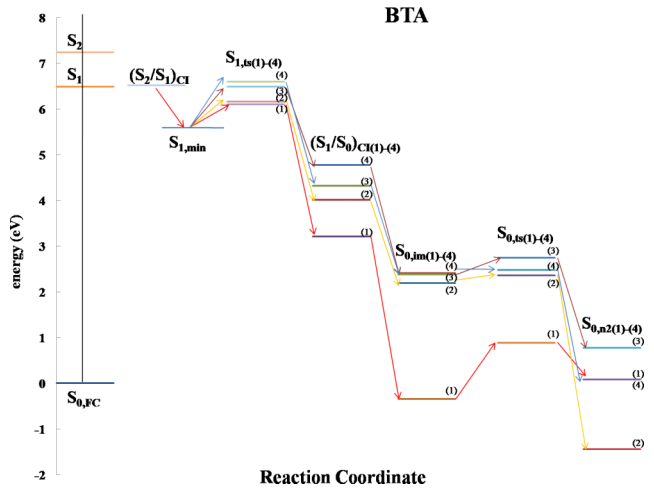

FIG. 13. A schematic one-dimensional projection of the multi-dimensional energy surfaces for four BTA dissociation paths computed at the CASSCF(12,8)/6-31G(d) level of theory. The four reaction paths contain four tetrazole ring opening channels. The red, orange, brown, and blue arrows represent (1)–(4) different reaction channels for N_2 dissociation, respectively. $S_{0,FC}$ is the optimized minimum energy of BTA on the S_0 state. $(S_1/S_0)_{CI(1)-(4)}$ are the conical intersections between the S_0 and S_1 states and (1)-(4) related to four conical intersections in different reaction paths. $S_{1,ts(1)-(4)}$ are the excited transition states on the S_1 surface between the minimum structure $S_{1,min}$ on the S_1 excited electronic state and the related conical intersections. $S_{0,im(1)-(4)}$ are the intermediate states on the S_0 state after $(S_1/S_0)_{CI(1)-(4)}$, and $S_{0,ts(1)-(4)}$ are the transition states on the S_0 surface following the intermediate states $S_{0,im(1)-(4)}$ in different reaction channels. $S_{0,n2(1)-(4)}$ are N_2 dissociated products on the S_0 surface.

eV, with the tetrazole ring opening between the N2—N3 and the N3—N4 bonds, respectively.

The adiabatic energy gaps between the S_1 and S_0 surfaces near conical intersections $(S_1/S_0)_{CI(1)-(4)}$ are computed to be in the range between 22 and 110 cm^{-1}, which means the S_1 and S_0 surfaces are strongly non-adiabatically coupled with one another: the small energy gap increases the probability of a non-adiabatic transition from the upper to lower electronic states. As the molecule moves from the S_1 to S_0 state through $(S_1/S_0)_{CI(1)-(4)}$, the IRC algorithm shows that the steepest descent pathway for the molecule is to evolve to stable intermediate states $S_{0,im(1)-(4)}$. From the IRC scan, the tetrazole ring remains open for the intermediate states $S_{0,im(1)-(4)}$ from $(S_1/S_0)_{CI(1)-(4)}$. The molecule then surmounts energy barriers in the range between 0.60 eV and 0.91 eV through the concerted transition states $S_{0,ts(1)(2)(4)}$ and forms N_2 products $S_{0,n2(1)(2)(4)}$. From intermediate state $S_{0,im(3)}$ on the third reaction path, there are two transition states on the way to form N_2 with energy barriers 4.62 eV ($S_{0,ts(3)a}$) and 2.74 eV ($S_{0,ts(3)b}$). Transition state $S_{0,ts(3)a}$ has a rectangular structure, and since its energy barrier is more than 1.5 eV higher compared to the transition states on the other three reaction channels, reaction path (3) (brown in Figure 9) is the least likely one. If the tetrazole ring opens on the ground electronic state S_0 to create an N_2 product, the energy barriers in this case will be greater than 3.5 eV; therefore, 1-DTE is more likely to open the tetrazole ring on the first excited state S_1 and then move to the S_0 state through various conical intersections. The N_2 product moves away from the rest of the molecule or radical without obvious torque for all the reaction channels as shown in Figure 10. Therefore, N_2 products should have low rotational temperatures, as is consistent with the experimental results. The energies of the final molecule with a dissociated N_2 product in the four reaction paths are in the range between −0.98 eV and 2.19 eV, which means these N_2 products should thereby have high vibrational temperatures based on the calculations.[25,26]

In sum, 1-DTE absorbs two laser photons and moves from the ground state to the high electronic states. It then decomposes to form N_2 products, following four possible reaction paths as shown in Figure 9. The tetrazole ring of 1-DTE opens on the first excited state S_1 and the N_2 product is dissociated on the ground electronic state potential energy surface. The decomposition dynamics are purely non-adiabatic in nature and the conical intersections can lead rapidly and efficiently to internal conversion from upper to lower electronic states through these non-adiabatic, radiationless transitions. Conical intersections are now firmly established to be the key features in the excited electronic state chemistry of energetic materials. During this internal conversion, electronic energy in the upper state is converted to vibrational energy in the lower state with a potential time scale of a few tens of femtoseconds. Thereby, the electronic excitation directly contributes to the 1-DTE ground state vibrational energy employed to break covalent chemical bonds. The difference between the excited state energy of 1-DTE and the energy of the final decomposition structure with an N_2 dissociated product plus their internal energies is the energy released from 1-DTE decomposition in this initial molecular step. Although we do not obtain the experimental vibrational temperature of the N_2 product, based on our theoretical calculation, N_2 should have a high vibrational temperature. This conclusion is consistent with our previous studies of energetic materials generating NO with high vibrational temperature.[21–36] In condensed phase, the explosion involves a chain reaction: this further reaction chain is not directly incorporated into the isolated molecule initial reaction mechanism, although it certainly depends upon the molecular mechanism and dynamics.[41] Consistent with a high product vibrational temperature, energy is stored in the initial decomposition products (N_2 and the rest of the energetic molecule), which can trigger secondary decomposition reactions in high density and condensed phase energetic systems.

Similar to previous studies of energetic bistetrazole materials (1,5′-BT and 5,5′-BT) without an NO_2 or N_2O_2 (nitramine) group or any other functional group, such as N_3, the tetrazole ring must be opened in order to form an initial small molecule, N_2 product. Totally four conical intersections are found on the 1-DTE potential surfaces between the S_0 and S_1 states related to four different tetrazole ring opening positions (mechanisms) and all of them can lead to the decomposition to an N_2 product. On the first excited state surface S_1, the N—N bond (especially the N1—N2 bond) on the tetrazole ring is less energy expensive to break than the C—N bond; however, enough energy is absorbed by the molecule in the multi photon decomposition process such that all four ring opening positions are energy available.

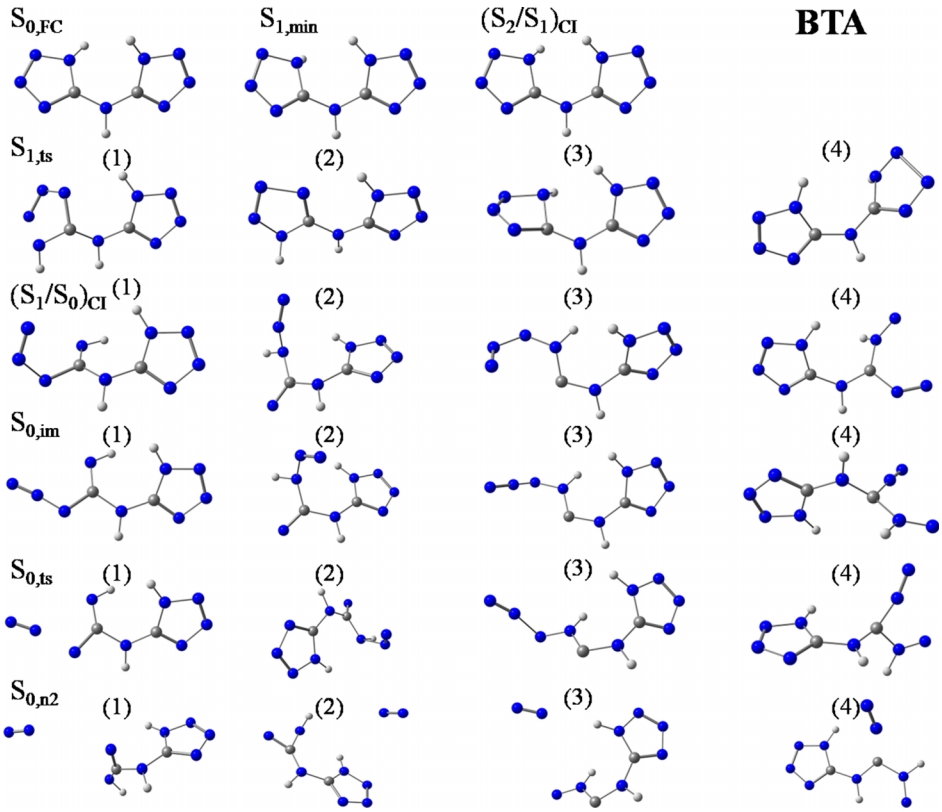

FIG. 14. Structures of all critical points and conical intersections mentioned in Figure 13 along the BTA dissociation reaction paths (1)-(4). For atoms in the structure, grey is carbon, blue is nitrogen, and white is hydrogen.

B. Potential energy surfaces for 5-DTE

Schematic one-dimensional projections of the multidimensional singlet potential energy surfaces (S_0 and S_1) of 5-DTE, with locations and potential energies for different critical points and conical intersections along the minimum energy reaction paths, are plotted in Figure 11, and the energy for each point is summarized in Table II. Similar to Figure 9 for 1-DTE, Figure 11 describes four different reaction channels for 5-DTE decomposition. The reaction coordinates depicted in Figure 11 include C—N and N—N bond lengths of the tetrazole ring of 5-DTE. Arrows with colors red, orange, brown, and black in Figure 11 indicate different possible decomposition channels: structures of these critical points are summarized in Figure 12. In Figures 11 and 12, FC geometry $S_{0,FC}$ is the optimized minimum energy of 5-DTE on the S_0 state and $(S_1/S_0)_{CI(1)-(4)}$ are the four conical intersections between the S_0 and S_1 states related to the four different reaction paths or decomposition mechanisms. $S_{1,ts(1)-(4)}$ are the transition states on the S_1 surface between the minimum structure $S_{1,min}$ and the related conical intersections. $S_{0,im(1)-(4)}$ are the intermediate states on the S_0 surface after $(S_1/S_0)_{CI(1)-(4)}$, and $S_{0,ts(1)-(4)}$ are the transition states on the S_0 surface following the intermediate states $S_{0,im(1)-(4)}$ in the different reaction channels. $S_{0,n2(1)-(4)}$ are N_2 dissociated products on the S_0 surface.

Reaction paths in Figure 11 show that, similar to 1-DTE, with two photon absorption, 5-DTE can be excited to an S_n ($n > 2$) excited state, and then it evolves to the first excited electronic state S_1 through several conical intersections. On the S_1 state, 5-DTE undergoes a rapid internal conversion to the energy minimum structure $S_{1,min}$. The molecule surmounts energy barriers to the transition states $S_{1,ts(1)-(4)}$ and moves to the ground electronic state surface S_0 through conical intersections $(S_1/S_0)_{CI(1)-(4)}$. Four transition states on the S_1 surface are identified for the four different conical intersections $(S_1/S_0)_{CI(1)-(4)}$: their energies are listed in Table II. The reaction path with the lowest transition state energy shown in Figure 11 is the red path (reaction path (1) in Figure 11 and Table II). On the red path coordinate, the molecule evolves from $S_{1,min}$, surmounts a 0.64 eV energy of $S_{1,ts(1)}$, and reaches the conical intersection $(S_1/S_0)_{CI(1)}$. Due to this lowest energy barrier, the red reaction path might be the most probable one for the system: the tetrazole ring then opens at the N1—N2 bond in this channel.

The energy barriers along the reaction paths (2)-(4) from $S_{1,min}$ to $(S_1/S_0)_{CI(2)-(4)}$ are 0.75, 0.89 and 1.23 eV, respectively: the tetrazole ring opening at the C—N bond encounters the second highest barrier. As all the transition states $S_{1,ts(1)-(4)}$ are energy accessible for the 2-photon absorption experimental system, all four reaction channels in 5-DTE are possible. The adiabatic energy gaps between S_1 and S_0 surfaces near $(S_1/S_0)_{CI(1)-(4)}$ are computed to be in the range between 24 and 57 cm^{-1}: the S_1 and S_0 surfaces are thereby strongly non-adiabatically coupled with one another and the small energy gaps increase the probability of non-adiabatic transitions from upper to lower electronic states.

As the molecule evolves from the S_1 to S_0 state through $(S_1/S_0)_{CI(1)-(4)}$, the IRC algorithm shows that the molecule moves to the stable intermediate states $S_{0,im(1)-(4)}$ while the tetrazole ring remains open. From $S_{0,im(1)-(4)}$, the molecule surmounts energy barriers in a range from 0.03 to 0.76 eV through the concerted transition states $S_{0,ts(1)-(4)}$ and forms N_2 products $S_{0,n2(1)-(4)}$. The N_2 product moves away from the whole molecule without obvious torque for all the reaction

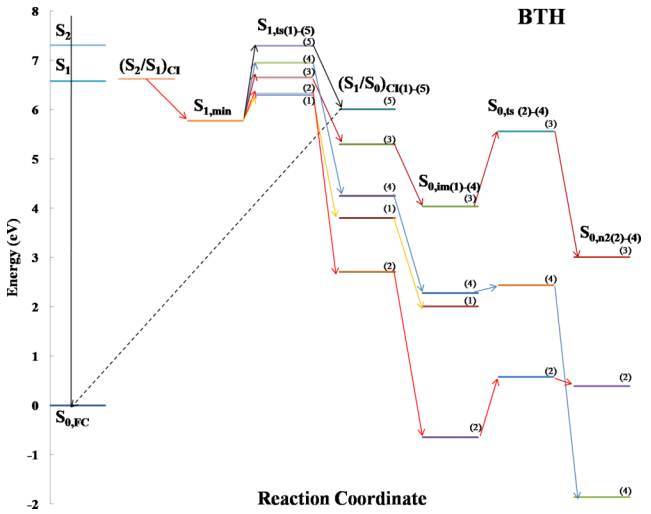

FIG. 15. A schematic one-dimensional projection of the multi-dimensional energy surfaces for five BTH dissociation path computed at the CASSCF(12,8)/6-31G(d) level of theory. The five reaction paths contain four tetrazole ring opening channels and one C—N bond breaks between tetrazole ring and the NH—NH link. The red, orange, brown, blue, and black arrows represent (1)–(5) different reaction channels for N_2 dissociation, respectively. $S_{0,FC}$ is the optimized minimum energy of BTH on the S_0 state with a planar structure. $(S_1/S_0)_{CI(1)-(5)}$ are the conical intersections between the S_0 and S_1 states and $S_{1,ts(1)-(5)}$ are the excited transition states on the S_1 surface between the minimum structure $S_{1,min}$ and the related conical intersections. $S_{0,im(1)-(4)}$ are the intermediate states on S_0 after $(S_1/S_0)_{CI(1)-(4)}$, and $(S_1/S_0)_{CI(5)}$ moves back to $S_{0,FC}$ after the IRC scan. $S_{0,ts(2)-(4)}$ are the transition states on the S_0 surface following the related intermediate states $S_{0,im(2)-(4)}$ in different reaction channels, while in channel (1) the reaction terminates at $S_{0,im(1)}$. $S_{0,n2(2)-(4)}$ are N_2 dissociated products on the S_0 state.

channels shown in Figure 11. Therefore, N_2 products should have low rotational temperatures, as is consistent with the experimental results. The energies of the final products with dissociated N_2 on the four reaction paths are between −0.30 eV and −1.49 eV (lower than the energy of $S_{0,FC}$), implying that these N_2 products should have a relatively high vibrational temperature.

In sum, 5-DTE absorbs two laser photons and is electronically excited in the experiment: it undergoes decomposition to form N_2 products, through four different reaction paths or mechanisms. Both 1-DTE and 5-DTE have two tetrazole rings linked by a CH_2—CH_2 bridge and similar to 1-DTE, the tetrazole ring of 5-DTE opens on the first excited state S_1, while the N_2 product is dissociated on the ground electronic state S_0. Conical intersections are the key features in the excited electronic state chemistry of organic molecules, in general, and energetic molecules in particular. The difference between the excited state energy of 5-DTE and the energy of the final decomposition structure with an N_2 dissociated product plus their internal energies is the energy released from energetic material decomposition in this initial molecular step. The energies of the final molecules with the N_2 decomposition product in 5-DTE are from −0.30 to −1.49 eV, which are lower than the dissociation products for 1-DTE (−0.98 to 2.19 eV). Since the UV-vis absorption wavelengths of 1-DTE and 5-DTE are extremely close (186–187 nm), more energy can be stored in the 5-DTE system. The N—N bond, especially the N1—N2 bond, of the tetrazole ring is the easiest one to break: the tetrazole ring opening from the C—N bond has the second highest energy barrier. The present results for 1(5)-DTE energetic molecules are similar to those found for 1,5′-BT and 5,5′-BT, which also have two bound tetrazole rings, in that the N1—N2 ring position is the lowest energy ring opening one for the generation of N_2 products.[26] This ring opening process for all four molecules occurs on the S_1 excited state surface, while the final release of N_2 occurs on the S_0 state potential energy surface.

C. Potential energy surfaces for BTA

Schematic one-dimensional projections of the multidimensional singlet potential energy surfaces (S_0 and S_1) of BTA, with locations and potential energies for different critical points and conical intersections along the minimum energy reaction paths, are plotted in Figure 13 and the energy for each point is summarized in Table III. As presented for 1-DTE and 5-DTE, arrows with colors in red, orange, brown, and blue in Figure 13 indicate different possible reaction channels or mechanisms for BTA initial decomposition. The molecular structures for BTA critical points and conical intersections are summarized in Figure 14. In Figures 13 and 14, FC geometry $S_{0,FC}$ is the optimized minimum energy on the S_0 state, $(S_1/S_0)_{CI(1)-(4)}$ are the conical intersections between the S_0 and S_1 states, and (1)-(4) relate to the different ring opening positions on the tetrazole ring in the different reaction channels. $S_{1,ts(1)-(4)}$ are the excited transition states on the S_1 surface between the minimum structure $S_{1,min}$ and the related conical intersections. $S_{0,im(1)-(4)}$ are the intermediate states on S_0 following $(S_1/S_0)_{CI}$, $S_{0,ts(1)-(4)}$ are the transition states on the S_0 surface following the intermediate states $S_{0,im(1)-(4)}$ in the different reaction channels, and $S_{0,n2(1)-(4)}$ are N_2 dissociated products on the S_0 state.

The reaction paths in Figure 13 show that, with two photon absorption, BTA can be excited to its S_n ($n > 2$) state and then evolve to the first excited electronic state S_1 through several conical intersections. On the S_1 state, BTA undergoes a rapid internal conversion to the energy minimum structure $S_{1,min}$. Next, the molecule encounters energy barriers to transition states $S_{1,ts(1)-(4)}$ and passes to the ground electronic state through the $(S_1/S_0)_{CI(1)-(4)}$ conical intersections: molecules undergoing these processes place sufficient vibrational energy in the S_0 state, transferred from the S_n electronic energy, to dissociate. The four transition states on the S_1 potential energy surface relate to, and lead to, four different conical intersections with different tetrazole ring openings: energies for these transition states are listed in Table III. Energy barriers from $S_{1,min}$ to the transition states are between 0.55 eV and 1.03 eV. Among these four reaction channels, the reaction path with the lowest transition state energy is the red one shown in Figure 13 (reaction path (1) in Figure 13 and Table III). On the red path, the molecule evolves from $S_{1,min}$, surmounts a 0.55 eV energy barrier to $S_{1,ts(1)}$ and then reaches conical intersection $(S_1/S_0)_{CI(1)}$ at which point the tetrazole ring opens at the N1—N2 bond, all on the S_1 excited state potential energy surface. The tetrazole ring opening from the C—N bond has the next higher energy barrier and is only 0.1 eV lower than ring opening at the N2—N3 bond. The adiabatic energy gaps between the S_1 and S_0 surfaces near $(S_1/S_0)_{CI(1)-(4)}$

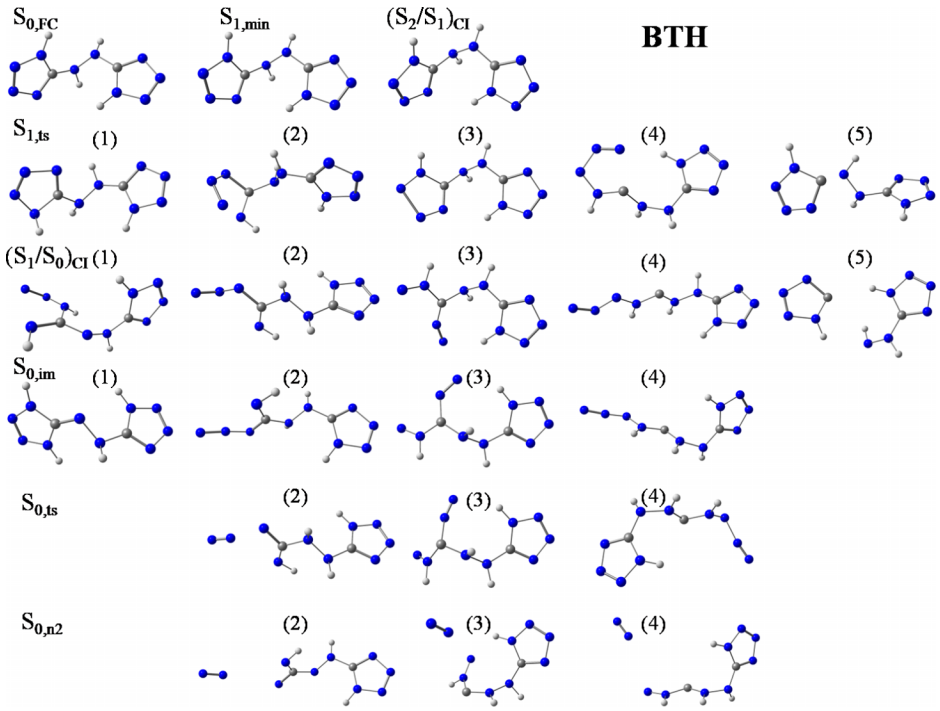

FIG. 16. Structures of all critical points and conical intersections mentioned in Figure 15 along the BTH dissociation reaction paths (1)-(5). For atoms in the structure, grey is carbon, blue is nitrogen, and white is hydrogen.

are computed to be in the range between 11 and 26 cm^{-1}; therefore, the S_1 and S_0 surfaces are strongly non-adiabatically coupled with one another. These small energy gaps increase the probability of non-adiabatic transition from upper to lower electronic states.

As the molecule moves from S_1 to S_0 through any of the $(S_1/S_0)_{CI(1)-(4)}$, it progresses on S_0 to the stable intermediate states $S_{0,im(1)-(4)}$, while the tetrazole ring remains open. From $S_{0,im(1)-(4)}$, the molecule surmounts energy barriers in the range from 0.07 to 1.23 eV through the concerted transition states $S_{0,ts(1)-(4)}$ and forms the N_2 products $S_{0,n2(1)-(4)}$. N_2 products move away from the remaining molecule without obvious torque for all the reaction channels shown in Figure 13. Therefore, N_2 products should have low rotational temperatures, as is consistent with the experimental results. Energies of the final molecule with dissociated N_2 product for the four reaction paths are in the range from −1.44 eV to 0.78 eV. The energy difference between the laser energy, which is the original molecule energy, and the energy of the final structure with N_2 products and their internal energies, is the energy released from BTA decomposition in its initial decomposition step. Additionally, based on the calculations, N_2 should have a high vibrational temperature.

In sum, BTA absorbs two laser photons and is electronically excited in the experiment: it undergoes decomposition to form N_2 products, through the four reaction paths shown in Figure 13. Conical intersections are the key features in the excited electronic state chemistry of organic molecules in general, and energetic molecules in particular. Since BTA has two tetrazole rings linked by an NH group, and its excitation energy and molecular structure are quite different from 1-DTE and 5-DTE, one cannot simply compare the energy of the final structure with an N_2 product to determine which energetic molecule stores more vibrational energy and has better explosive performance. Moreover, in the condensed phase, decomposition reactions occur within the confines of the rigid constraining environment of a crystal lattice, in which intermolecular interactions can influence reaction mechanisms and directions.[39] Energies calculated for an isolated molecule can be affected by these intermolecular interactions: these latter interactions can influence (chain) reactions following the initial molecular one and thereby can influence condensed phase explosive performance. Nonetheless, the lowest energy mechanism to open the tetrazole ring for these nitrogen rich energetic molecules is through rupture of the N1—N2 bond. This generalization is apparently true independent of the bridging group between the two rings; however, as the energy barriers to break the N—N and C—N bonds of the tetrazole ring of BTA are not very different, all pathways are within the molecular energy limit and all of them are available within the experimental conditions.

BTA is found to have better explosive performance than RDX (detonation velocity, $D_{BTA} \sim 9120$ m/s > $D_{RDX} \sim 8800$ m/s).[9] Comparison of the energy release behavior and

TABLE I. Summary of reaction paths and critical point energies for the 1-DTE decomposition reaction.

Reaction path	Color	$S_{1,ts}$	$(S_1/S_0)_{CI}$	$S_{0,im}$	$S_{0,ts}$	$S_{0,im(b)}$	$S_{0,ts(b)}$	$S_{0,n2}$
(1)	Red	5.80	3.27	0.21	1.12	/	/	0.64
(2)	Orange	6.65	4.29	2.20	2.80	/	/	2.18
(3)	Brown	7.06	4.14	2.19	4.62	1.89	2.74	−0.98
(4)	Blue	7.07	5.78	2.98	3.64	/	/	2.19

Details of each reaction path (i)	
i = 1, 2, 4	$S_{min} \rightarrow S_{1,ts(i)} \rightarrow (S_1/S_0)_{CI(i)} \rightarrow S_{0,im(i)} \rightarrow S_{0,ts(i)} \rightarrow S_{0,n2(i)}$
i = 3	$S_{min} \rightarrow S_{1,ts(i)} \rightarrow (S_1/S_0)_{CI(i)} \rightarrow S_{0,im(a)} \rightarrow S_{0,ts(a)} \rightarrow S_{0,im(b)} \rightarrow S_{0,ts(b)} \rightarrow S_{0,n2(i)}$

TABLE II. Summary of reaction paths and critical point energies for the 5-DTE decomposition reaction.

Reaction path	Color	$S_{1,ts}$	$(S_1/S_0)_{CI}$	$S_{0,im}$	$S_{0,ts}$	$S_{0,n2}$
(1)	Red	4.57	1.86	−1.64	−0.88	−1.13
(2)	Orange	4.68	2.48	0.47	0.86	−1.49
(3)	Brown	4.82	4.41	0.67	1.16	−0.35
(4)	Blue	5.16	2.57	0.69	0.72	−0.30
Details of each reaction path (i = 1-4)						
$S_{min} \rightarrow S_{1,ts(i)} \rightarrow (S_1/S_0)_{CI(i)} \rightarrow S_{0,im(i)} \rightarrow S_{0,ts(i)} \rightarrow S_{0,n2(i)}$						

mechanisms of BTA with those of BTH will be made in Subsection V D. BTA and BTH are more easily compared to one another than they can be to 1(5)-DTE, due to structural and electronic similarities: BTA can be argued to be a more efficient energy storage system than BTH.

D. Potential energy surfaces for BTH

Schematic one-dimensional projections of the multidimensional singlet potential energy surfaces (S_0 and S_1) of BTH, with locations and potential energies for different critical points and conical intersections along the minimum energy reaction paths, are plotted in Figure 15 and the energy for each point is summarized in Table IV. Figure 15 describes five different reaction mechanisms or channels for BTH decomposition. The reaction coordinates depicted in Figure 15 include C—N and N—N bond lengths at the BTH active sites. These sites include the tetrazole ring opening positions and the breaking of the C—N bond between the tetrazole ring and the NH—NH structure joining the rings. Arrows with colors in red, orange, brown, blue, and black in Figure 15 indicate different possible reaction channels or mechanisms for BTH decomposition. The structures of each critical point and conical intersection are summarized in Figure 16. In Figures 15 and 16, FC geometry $S_{0,FC}$ is the optimized minimum energy of BTH on the S_0, $(S_1/S_0)_{CI(1)-(5)}$ are the conical intersections between the S_0 and S_1 potential energy surfaces, and (1)-(5) relate to the five different decomposition channels. $S_{1,ts(1)-(5)}$ are the excited transition states on the S_1 surface between the minimum structure $S_{1,min}$ and the related conical intersections. $S_{0,im(1)-(4)}$ are the intermediate states on S_0 subsequent to the $(S_1/S_0)_{CI}$, and $S_{0,ts(2)-(4)}$ are the transition states on the S_0 surface following the related intermediate states in the different reaction channels. Labels (1) and (5) for $S_{0,ts}$ and label (5) for $S_{0,im}$ are missing because the first reaction path terminates in $S_{0,im(1)}$, and the fifth one goes back to the $S_{0,FC}$ structure following the conical intersection $(S_1/S_0)_{CI(5)}$. $S_{0,n2(2)-(4)}$ are N_2 dissociated products on the S_0 potential energy surface.

TABLE III. Summary of reaction paths and critical point energies for the BTA decomposition reaction.

Reaction path	Color	$S_{1,ts}$	$(S_1/S_0)_{CI}$	$S_{0,im}$	$S_{0,ts}$	$S_{0,n2}$
(1)	Red	6.11	3.21	−0.34	0.89	0.08
(2)	Orange	6.17	4.02	2.19	2.36	−1.44
(3)	Brown	6.49	4.77	2.39	2.74	0.78
(4)	Blue	6.60	4.32	2.41	2.48	0.08
Details of each reaction path (i = 1-4)						
$S_{min} \rightarrow S_{1,ts(i)} \rightarrow (S_1/S_0)_{CI(i)} \rightarrow S_{0,im(i)} \rightarrow S_{0,ts(i)} \rightarrow S_{0,n2(i)}$						

TABLE IV. Summary of reaction paths and critical point energies for the BTH decomposition reaction.

Reaction path	Color	$S_{1,ts}$	$(S_1/S_0)_{CI}$	$S_{0,im}$	$S_{0,ts}$	$S_{0,n2}$
(1)	Orange	6.29	3.80	2.01	/	/
(2)	Red	6.32	2.71	−0.65	0.58	0.39
(3)	Brown	6.65	5.29	4.03	5.55	3.01
(4)	Blue	6.94	4.24	2.28	2.43	−1.86
(5)	Black	7.29	6.01 (back to $S_{0,FC}$)			
Details of each reaction path (i = 1-4)						
i = 1	$S_{min} \rightarrow S_{1,ts(i)} \rightarrow (S_1/S_0)_{CI(i)} \rightarrow S_{0,im(i)}$					
i = 2-4	$S_{min} \rightarrow S_{1,ts(i)} \rightarrow (S_1/S_0)_{CI(i)} \rightarrow S_{0,im(i)} \rightarrow S_{0,ts(i)} \rightarrow S_{0,n2(i)}$					
i = 5	$S_{min} \rightarrow S_{1,ts(i)} \rightarrow (S_1/S_0)_{CI(i)} \rightarrow S_{0,FC}$					

The reaction paths in Figure 15 show that, with two photon absorption, BTH can be excited to its S_n ($n > 2$) state and then evolve to the first excited electronic state S_1 through several conical intersections. On the S_1 state, BTH undergoes a rapid internal conversion to the energy minimum structure $S_{1,min}$. Next, the molecular evolution encounters energy barriers to transition states $S_{1,ts(1)-(5)}$ as the molecule passes to the ground electronic state through the $(S_1/S_0)_{CI(1)-(5)}$ conical intersections: molecules undergoing this process place sufficient vibrational energy in the S_0 state, transferred from the S_n electronic excitation energy, to dissociate. The five transition states on the S_1 potential energy surface are related to four different tetrazole ring opening positions, in addition to cleavage of the bond between the tetrazole ring and the NH—NH link. The energies of these transition states are listed in Table IV: energy barriers from $S_{1,imn}$ to the transition states are from 0.52 eV to 1.52 eV. Among these five reaction channels, the breaking of N3—N4 bond (reaction path (1), orange) and N1—N2 bond (reaction path (2), red) has the lowest energy barriers. On the reaction paths (1) and (2), the molecule moves from $S_{1,min}$, surmounts a 0.52 eV (0.55 eV) energy barrier to $S_{1,ts(1)}$ ($S_{1,ts(2)}$) and then reaches conical intersection $(S_1/S_0)_{CI(1)}$ ($(S_1/S_0)_{CI(2)}$). The energy barrier for the tetrazole ring opening at the C—N bond is higher than that for the N—N bond (1.17 eV). The breaking of the C—N bond between the tetrazole ring and the NH—NH link without ring opening has the highest energy barrier (1.52 eV). The adiabatic energy gaps between the S_1 and S_0 surfaces near $(S_1/S_0)_{CI(1)-(5)}$ are computed to be in the range between 28 and 199 cm^{-1}; therefore, the S_1 and S_0 adiabatic surfaces are strongly non-adiabatically coupled with one another, as a small energy gap increases the probability of a non-adiabatic transition from upper to lower electronic states.

As the molecule transitions from the S_1 to S_0 state through $(S_1/S_0)_{CI(1)-(5)}$, the steepest descent pathways for the molecule are to evolve to either the stable intermediate states

$S_{0,im(1)-(4)}$ or to the Frank-Condon structure $S_{0,FC}$. Based on the IRC scan, conical intersection $(S_1/S_0)_{CI(5)}$ without the tetrazole ring opening returns to the Frank-Condon structure. Again following the IRC scan, although $(S_1/S_0)_{CI(1)}$ does not go back to the Frank Condon minimum energy structure, its tetrazole ring closes. To reopen the tetrazole ring, the energy barrier is more than 3 eV on the ground electronic state S_0; on this pathway, formation of the N_2 product on the ground state has a low probability. From $S_{0,im(2)-(4)}$, the molecule surmounts energy barriers in the range from 0.15 to 1.52 eV through the concerted transition states $S_{0,ts(2)-(4)}$ and forms N_2 products $S_{0,n2(2)-(4)}$. N_2 products move away from the remaining molecule without obvious torque for all the reaction channels shown in Figure 15. Therefore, N_2 products should have low rotational temperatures, as is consistent with the experimental results. Energies of the final molecules with dissociated N_2 for the four reaction paths are in the range −1.86 to 3.01 eV. The energy difference between the laser energy, which is the original molecule energy, and the energy of the final structure with N_2 products and their internal energies, is the energy released from BTH decomposition in its initial decomposition step. Based on the theoretical calculation, N_2 should have a high vibrational temperature.

In sum, BTH absorbs two laser photons and is electronically excited in the experiment: it undergoes decomposition to form an N_2 product, through three reaction paths as shown in Figure 15. Conical intersections are the key features in the excited electronic state chemistry of organic molecules in general, and energetic molecules in particular. Compared to BTA, BTH has one more NH group between the two tetrazole rings. Our calculations reveal that BTH has one less reaction channels for the creation of an N_2 product; additionally, the final molecules with N_2 product from BTH have relatively higher energy (−1.86 eV to 3.01 eV) compared to the final products in BTA (−1.44 eV to 0.78 eV). In this case, more vibrational energy can be stored for further dissociation reaction in BTA than BTH. This conclusion is consistent with a previous study indicating that BTA has better explosive performance than BTH.[19] Note that for 1-DTE, 5-DTE, BTA, 1,5′-BT, and 5,5′-BT (all nitrogen-rich energetic materials with tetrazole rings), the most active bond to open the tetrazole ring forming an N_2 product is the N1—N2 bond no matter how the tetrazole rings are connected to each other.[26] The C—N bond on the tetrazole ring is more energy expensive to break than the N—N bond. Under the experimental conditions employed, all N—N and C—N bonds of the tetrazole ring can open for further decomposition reactions. Although BTH can decompose at its NH—NH link, the tetrazole ring is more reactive for formation of an N_2 product.

Transition state energy barriers for N—N bond fission of the tetrazole ring on the S_1 states of 1-DTE and 5-DET are 5.80 eV and 4.57 eV, respectively: these barriers are lower than the transition state energy barriers for BTA and BTH which are 6.11 eV and 6.29 eV, respectively. Previous measurements of the detonation velocity D (m/s) for the four energetic materials are D_{DTE} ~ 7219 m/s, lower than D_{BTA} and D_{BTH}, which are around 8523 to 9120 m/s. These values imply that BTA and BTH have better explosive performance than do 1-DTE and 5-DTE.[7,12,19] The detonation is a condensed phase property and in the solid state, the presence of intermolecular interactions, solvates, planar defects, phase transitions, disorder, and even crystal morphology can all affect the decomposition properties.[39,42] Thus one cannot readily determine which energetic material has better explosive performance by simply comparing their gas phase decomposition energy barriers on the first excited electronic state. As shown in the UV-vis spectra of Figure 6, BTA and BTH have excited states in the range from 182 nm to 230 nm, while for 1-DTE and 5-DTE the excitation range is narrower (from 182 to 200 nm). Since 1(5)-DTE excitation is more restricted than that for BTA and BTH, this difference could be related to their explosive property difference. The two tetrazole rings of 1-DTE and 5-DTE are connected by a CH_2—CH_2 group, while for BTA and BTH, they are connected by an NH or NH—NH group. The difference of the structures between tetrazole rings can cause apparent differences in explosive behavior among the different energetic materials, as well.

From our previous studies of other types of energetic molecules, the N_2 product observed from energetic salts TKX-50 and MAD-X1[25] and nitrogen-rich energetic molecules 1,5′-BT, 5,5′-BT, and AzTT,[26] always has a low rotational temperature and a high calculated vibrational temperature. The behavior of the N_2 product from 1-DTE, 5-DTE, BTA, and BTH is consistent with the behavior of previous energetic compounds reported. The vibrational temperature of the initial dissociation product is important in recognizing energetic molecules because initial decomposition products with high vibrational excitation are better able to propagate a chain reaction following the initial stimulus, leading to detonation. With vibrationally hot N_2 as an initial dissociation product, the energetic properties of 1-DTE, 5-DTE, BTA, and BTH are similar in behavior to the older energetic materials.[21–36] The $S_n \rightarrow \cdots \rightarrow S_o$ pathways through a series of conical intersections leaves the molecule on a new part of the S_0 potential energy surface, not necessarily near the FC equilibrium point.[30,31] Thereby, all the excitation energy is available to break internal bonds to generate reactive fragments and radicals for further reactions as required to classify a high energy molecule as a potential energetic material.

VI. CONCLUSIONS

Decomposition of the nitrogen rich energetic materials 1-DTE, 5-DTE, BTA, and BTH following electronic excitation has been explored. These materials create N_2 as initial decomposition products through a number of distinct reaction channels. The rotational temperature of N_2 products from all four tetrazole ring based energetic molecule is cold (<30 K). Based on the experimental observations and CASSCF calculations, the N_2 products are released by the opening of tetrazole ring of all four energetic molecule. The tetrazole ring opens on the S_1 excited state surfaces, and through conical intersections $(S_1/S_0)_{CI}$, N_2 products are formed on the ground state surface with little rotational excitation at the last N_2 dissociation step. The tetrazole rings of all four energetic molecule, open at the N1—N2 bond with a lower energy

barrier than that of the C—N bond. BTH has a NH—NH bridge structure between the two tetrazole rings, which is less active than the tetrazole ring openings for N_2 formation. The vibrational temperatures of N_2 products from all four energetic molecules should be hot based on calculations. 1-DTE and 5-DTE have two tetrazole rings connected by CH_2—CH_2 groups; BTA and BTH have tetrazole groups connected by NH or NH—NH groups. The different groups between tetrazole rings can cause apparent difference in explosive behavior among different energetic materials. Conical intersections are the key point for the theoretically derived mechanisms, as they provide non-adiabatic, ultrafast radiationless internal conversion between upper and lower electronic states on the fs time scale, and place the undissociated molecule on a new part of the ground state potential surface with all its excitation energy placed in the ground state vibrations available for bond breaking.

ACKNOWLEDGMENTS

This study is supported by a grant from the U.S. Army Research Office (ARO, Grant Nos. FA9550-10-1-0454 and W911-NF13-10192) and in part by the U.S. National Science Foundation (NSF) through the XSEDE supercomputer resources provided by NCSA under Grant No. TG-CHE110083. We also want to thank Professor Dr. Thomas M. Klapötke, Ludwig-Maximilian University of Munich for supplying the 1-DTE, 5-DTE, BTA, and BTH samples used in this study and for helpful advice on their properties and handling.

[1]M. Liu, S. Cheng, K. Cheng, and C. Chen, "Kinetics of decomposition pathways of an energetic GZT molecule," Int. J. Quantum Chem. **108**, 482 (2008).

[2]P. Politzer, M. E. Grice, and J. M. Seminario, "Density functional analysis of a decomposition of 4-nitro-1,2,3-triazole through the evolution of N_2," Int. J. Quantum Chem. **61**, 389 (1997).

[3]R. V. Tsyshevsky and M. M. Kuklja, "Decomposition mechanisms and kinetics of novel energetic molecules BNFF-1 and ANFF-1: Quantum-chemical modeling," Molecules **18**, 8500 (2013).

[4]D. Fischer, T. M. Klapotke, D. G. Piercey, and J. Stierstorfer, "Synthesis of 5-Aminotetrazole-1N-oxide and its Azo derivative: A key step in the development of new energetic materials," Chem. - Eur. J. **19**, 4602 (2013).

[5]H. Gao and J. M. Shreeve, "Azole-based energetic salts," Chem. Rev. **111**, 7377 (2011).

[6]J. Evers, I. Gospodinov, M. Joas, T. M. Klapotke, and J. Stierstorfer, "Cocrystallization of photosensitive energetic copper(II) perchlorate complexes with the nitrogen-rich ligand 1,2-di(1H-tetrazol-5-yl)ethane," Inorg. Chem. **53**, 11749 (2014).

[7]T. M. Klapotke and C. M. Sabate, "Bistetrazoles: Nitrogen-rich, high-performing, insensitive energetic compounds," Chem. Matter. **20**, 3629 (2008).

[8]M. Joas, T. M. Klapotke, and N. Szimhardt, "Photosensitive metal(II) perchlorates with 1,2-bis[5-(1-methylhydrazinyl)tetrazol-1-yl]ethane as ligand: Synthesis, characterization and laser ignition," Eur. J. Inorg. Chem. **3**, 493 (2014).

[9]T. M. Klapotke, P. Mayer, J. Stierstorfer, and J. J. Weig, "Bistetrazolyamins-synthesis and characterization," J. Matter. Chem. **18**, 5248 (2008).

[10]D. Laniel, E. Sebastiao, C. Cook, M. Murugesu, A. Hu, F. Zhang, and S. Desgreniers, "Debse nitrogen-rich energetic materials: A study of 5,5'-bis(1H-tetrazolyl)amine," J. Chem. Phys. **140**, 184701 (2014).

[11]C.-F. Qiao, C.-S. Zhou, Q. Wei, and Z.-Q. Xia, "A new polymorph of 5,5'-(ethane-1,2-diyl)bis(1H-tetrazole)," Acta Crystallogr., Sect. E: Struct. Rep. Online **68**, o989 (2012).

[12]L. S. Kovacevic, T. M. Klapotke, and S. M. Sproll, "Synthesis of a one-dimensional coordination polymer based on copper(II) nitrate and 1,2-bis(5-monomethylhydrazinyl-1H-tetrazolyl)ethane," Z. Anorg. Allg. Chem. **636**, 1079 (2010).

[13]L. Shen, J. Yang, G.-W. Yang, Q.-Y. Li, X.-Y. Tang, F. Zhou, and Z.-F. Miao, "Three novel coordination networks dependent upon H_2btze ligand [H_2btze = 1,2-bis(tetrazol-5-yl)ethane]," Inorg. Chim. Acta **370**, 150 (2011).

[14]Y. Guo, G.-H. Tao, Z. Zeng, H. Gao, D. A. Parrish, and J. M. Shreeve, "Energetic salts based on monoanions of N,N-bis(1H-tetrazol-5-yl)amine and 5,5'-bis(tetrazole)," Chem. Eur. J. **16**, 3753 (2010).

[15]L.-L. Dong, L. He, H.-Y. Liu, G.-H. Tao, F.-D. Nie, M. Huang, and C.-W. Hu, "Nitrogen-rich energetic ionic liquids based on the N,N-bis(1H-tetrazol-5-yl)amine anion-synthesis, structures and properties," Eur. J. Inorg. Chem. **2013**, 5009 (2013).

[16]M. Friedrich, J. C. Galvez-Ruiz, T. M. Klapotke, P. Mayer, B. Weber, and J. J. Weigand, "BTA copper complexes," Inorg. Chem. **44**, 8044 (2005).

[17]Y. Guo, H. Gao, B. Twamley, and J. M. Shreeve, "Energetic nitrogen rich salts of N,N-bis[1(2)H-tetrazol-5-yl]amine," Adv. Mater. **19**, 2884 (2007).

[18]G. Om Reddy and A. K. Chatterjee, "A study on thermal and explosive properties of hydrazotetrazoles," J. Hazard. Mater. **9**, 291 (1984).

[19]T. M. Klapotke and J. Stierstorfer, "High-nitrogen compounds for use in low-erosivity gun propellants," in 26th Proceedings of the Army Science Conference, Orlando, Florida, 1–4 December 2008.

[20]D. Yaempongsa, "Quantum chemical studies of new energetic molecules," M.S. thesis in physical chemistry in KTH Kemivetenskap, 2012, online version: http://www.diva-portal.se/smash/get/diva2:720739/FULLTEXT01.pdf.

[21]A. Bhattacharya, Y. Q. Guo, and E. R. Bernstein, "Nonadiabatic reactions of energetic molecules," Acc. Chem. Res. **43**, 1476 (2010).

[22]Y. Q. Guo, A. Bhattacharya, and E. R. Bernstein, "Decomposition of nitramine energetic materials in excited electronic states: RDX and HMX," J. Chem. Phys. **122**, 244310 (2005).

[23]Y. Q. Guo, M. Greenfield, A. Bhattacharya, and E. R. Bernstein, "On the excited electronic state dissociation of nitramine energetic materials and model systems," J. Chem. Phys. **127**, 154301 (2007).

[24]A. Bhattacharya and E. R. Bernstein, "Nonadiabatic decomposition of gas-phase RDX through conical intersections: An ONIOM-CASSCF study," J. Phys. Chem. A **115**, 4135 (2011).

[25]B. Yuan, Z. Yu, and E. R. Bernstein, "Initial mechanisms for the decomposition of electronically excited energetic salts: TKX-50 and MAD-X1," J. Phys. Chem. A **119**, 2965 (2015).

[26]B. Yuan, Z. Yu, and E. R. Bernstein, "Initial mechanisms for the decomposition of electronically excited energetic materials: 1,5'-BT, 5,5'-BT and AzTT," J. Chem. Phys. **142**, 124315 (2015).

[27]A. Bhattacharya, Y. Q. Guo, and E. R. Bernstein, "Unimolecular decomposition of tetrazine-N-oxide based high nitrogen content energetic materials from excited electronic states," J. Chem. Phys. **131**, 194304 (2009).

[28]A. Bhattacharya, Y. Q. Guo, and E. R. Bernstein, "Experimental and theoretical exploration of the initial steps in the decomposition of a model nitramine energetic material: Dimethylnitramine," J. Phys. Chem. A **113**, 811 (2009).

[29]Z. Yu and E. R. Bernstein, "Decomposition of pentaerythritoltetranitrate [$C(CH_2ONO_2)_4$] following electronic excitation," J. Chem. Phys. **135**, 154305 (2011).

[30]Z. Yu and E. R. Bernstein, "Experimental and theoretical studies of the decomposition of new imidazole based energetic materials: Model systems," J. Chem. Phys. **137**, 114303 (2012).

[31]Z. Yu and E. R. Bernstein, "On the decomposition mechanisms of new imidazole-based energetic materials," J. Phys. Chem. **117**, 1756 (2013).

[32]Y. Q. Guo, A. Bhattacharya, and E. R. Bernstein, "Decomposition of excited electronic state s-tetrazine and its energetic derivatives," J. Chem. Phys. **134**, 024318 (2011).

[33]Y. Q. Guo, A. Bhattacharya, and E. R. Bernstein, "Excited electronic state decomposition of furazan based energetic materials: 3,3′-Diamino-4,4′-azoxyfurazan and its model systems, diaminofurazan and furazan," J. Chem. Phys. **128**, 034303 (2008).

[34]Y. Q. Guo, A. Bhattacharya, and E. R. Bernstein, "Ultrafast S_1 to S_0 internal conversion dynamics for dimethylnitramine through a conical intersection," J. Phys. Chem. A **115**, 9349 (2011).

[35]B. Yuan, Z. Yu, and E. R. Bernstein, "Azole energetic materials: Initial mechanisms for the energy release from electronical excited nitropyrazoles," J. Chem. Phys. **140**, 034320 (2014).

[36]B. Yuan, Z. Yu, and E. R. Bernstein, "Initial decomposition mechanism for the energy release from electronically excited energetic materials: FOX-7 (1,1-diamino-2,2-dinitroethene, $C_2H_4N_4O_4$)," J. Chem. Phys. **140**, 074708 (2014).
[37]J. L. Maienschein, A. L. Nichols III, J. E. Reaugh, M. E. McClelland, and P. C. Hsu, "Hazards response of energetic materials-initiation mechanisms experimental characterization, and development of predictive capability," in 36th Internation ICT Conference, Karlsruhe, Germany, UCRL-CONF-211434, 2005.
[38]F. Toda, "Solid state organic chemistry: Efficient reactions, remarkable yields, and stereoselectivity," Acc. Chem. Res. **28**, 480 (1995).
[39]F. M. Nareetsile, Solventless isomerisation reactions of six-coordinate complexes of ruthenium and Molybdenum, Chapter two, Solid state reactions, 2006, online version: http://wiredspace.wits.ac.za/bitstream/handle/10539/1654/Chapter%202-%20Final.pdf?sequence=2&isAllowed=y.
[40]F. J. Owens, "Calculation of energy barriers for bond rupture in some energetic molecules," J. Mol. Struct.: THEOCHEM **370**, 11 (1996).
[41]D. Furman, R. Kosloff, F. Dubnikova, S. V. Zybin, W. A. Goddard III, N. Rom, B. Hirshberg, and Y. Zeiri, "Decomposition of condensed phase energetic materials: Interplay between uni- and bimolecular mechanisms," J. Am. Chem. Soc. **136**, 4192 (2014).
[42]A. L. Ramaswamy, "Microscopic initiation mechanisms in energetic material crystals," J. Energ. Mater. **2**, 195 (2001).
[43]D. D. Dlott and M. D. Fayer, "Shocked molecular solids: Vibrational uppumping, defect hot spot formation, and the onset of chemistry," J. Chem. Phys. **92**, 3798 (1990).
[44]G. E. Hardy, J. C. Baldwin, J. I. Zink, W. C. Kaska, P.-H. Liu, and L. Dubois, "Triboluminescence spectroscopy of aromatic compounds," J. Am. Chem. Soc. **99**, 3533 (1977).
[45]J. I. Zink and W. C. Kaska, "Triboluminescence of Hexaphenylcarbodiphosphorane: Emission from a molecular excited state populated by mechanical stress," J. Am. Chem. Soc. **95**, 7510 (1973).
[46]J. I. Zink, G. E. Hardy, and J. E. Sutton, "Triboluminescence of sugars," J. Phys. Chem. **80**, 248 (1976).
[47]J. I. Zink and W. Klimt, "Triboluminescence of coumarin. Fluorescence and dynamic spectral features excited by mechanical stress," J. Am. Chem. Soc. **96**, 4690 (1974).
[48]W. Beese and J. I. Zink, "Intensity of triboluminescence," J. Lumin. **29**, 119 (1984).
[49]G. E. Hardy and J. I. Zink, "Triboluminescence and pressure dependence of the photoluminescence of tetrahedral manganese (II) complexes," Inorg. Chem. **15**, 3061 (1976).
[50]S. H. Lin, D. Wutz, Z. Z. Ho, and H. Eyring, "Mechanisms of triboluminescence," Proc. Natl. Acad. Sci. U. S. A. **77**, 1245 (1980).
[51]M. M. Kuklja, "Role of electronic excitations in explosive decomposition of solids," J. Appl. Phys. **89**, 4156 (2001).
[52]E. J. Reed, J. D. Joannopoulos, and L. E. Fried, "Electronic excitations in shocked nitromethane," Phys. Rev. B. **62**, 16500 (2000).
[53]K. Takatsuka, T. Yonehara, K. Hanasaki, and Y. Arasaki, *Chemical Theory Beyond the Born-Oppenheimer Paradigm: Nonadiabatic Electronic and Nuclear Dynamics in Chemical Reactions* (World Scientific Publishing Co. Pte. Ltd, Singapore, 2015).
[54]W. Domcke, D. R. Yarkony, and H. Koppel, *Conical Intersections: Electronic Structure Dynamics and Spectroscopy*, Advanced Series in Physical Chemistry Vol. 15 (World Scientific Publishing Co. Pte. Ltd, Singapore, 2004).
[55]K. L. Carleton, K. H. Welge, and S. R. Leone, "Detection of nitrogen rotational distributions by resonant 2+2 multiphoton ionization through the $a^1\Pi_g$ state," Chem. Phys. Lett. **115**, 492 (1985).
[56]G. O. Sitz, A. C. Kummel, and R. N. Zare, "Population and alignment of N_2 scattered from Ag(111)," J. Vac. Sci. Technol., A **5**, 513 (1987).
[57]F. J. Aoiz, L. Banares, V. J. Herrero, B. Martinez-Haya, M. Menendez, P. Quintana, L. Tanarro, and E. Verdasco, "Low-temperature rotational relaxation of N_2 in collisions with Ne," J. Phys. Chem. A **105**, 6976 (2011).
[58]H. Mori, T. Ishida, Y. Aoki, and T. Niimi, "Spectroscopic study of REMPI for rotational temperature measurement in highly rarefied gas," AIP Conf. Proc. **585**, 956 (2001).
[59]Q. Gu, C. Trindle, and J. L. Knee, "Communication: Frequency shifts of an intramolecular hydrogen bond as a measure of intermolecular hydrogen bond strengths," J. Chem. Phys. **137**, 091101 (2012).
[60]E. H. Strickland, M. Wilchek, J. Horwitz, and C. Billups, "Effects of hydrogen bonding and temperature upon the near ultraviolet circular dichroism and absorption spectra of tyrosine and *O*-Methyl tyrosine derivatives," J. Biol. Chem. **247**, 572 (1972), http://www.jbc.org/content/247/2/572.long.
[61]A. T. Rhys Williams, An Introduction to Fluorescence Spectroscopy (PerkinElmer Inc., 1981), available on website: http://www.chem.uci.edu/~dmitryf/manuals/Fundamentals/Fluorescence%20Spectroscopy.pdf.